JGR Oceans

RESEARCH ARTICLE
10.1029/2024JC021753

Physical Connectivity Between Mesophotic Areas in the Northern Gulf of Mexico

Luisa Lopera[1,2], **Annalisa Bracco**[1,2], **and Santiago Herrera**[3]

[1]School of Earth and Atmospheric Sciences, Georgia Institute of Technology, Atlanta, GA, USA, [2]Program in Ocean Science and Engineering, Georgia Institute of Technology, Atlanta, GA, USA, [3]Department of Biological Sciences, Lehigh University, Bethlehem, PA, USA

Abstract Understanding connectivity patterns is crucial for marine planning, particularly in the design of marine protected areas or restoration plans. In this study, we assess the potential physical connectivity between mesophotic areas in the northern Gulf of Mexico and investigate the dynamical features influencing such connectivity using a physical modeling approach. We use the Coastal and Regional Ocean COmmunity model in conjunction with a particle transport Lagrangian tool to evaluate the general pathways of material transport among mesophotic areas, focusing on the Flower Garden Banks National Marine Sanctuary and the Pinnacles Trend over 2 years. Additionally, we conduct a sensitivity analysis to identify the minimum necessary model configuration for capturing the impact of kilometer-scale circulation on connectivity metrics. Our results reveal year-round low connectivity potential between mesophotic areas with high seasonal heterogeneity in transport direction and dispersal distances due to the high variability of the currents fields. In the study areas, material dispersion appears to be primarily driven by the extension of shelf currents and by submesoscale circulations (SCs). Sensitivity analysis suggests that high-resolution velocity fields with horizontal grid spacing capable of resolving SCs and temporal resolution of 6 hr or less are required to accurately capture the impact of small-scale circulations on connectivity, especially in summer, when currents are weak and submesoscale fronts are essential to establish dispersion patterns.

Plain Language Summary Transport by ocean currents at kilometer scale (submesoscales) is important for understanding connectivity among nearby reef ecosystems. In this study, we examine how areas known to host mesophotic corals at depths between 40 and 150 m can exchange material in the northern Gulf of Mexico using a three-dimensional ocean model and a particle tracking tool. Our goal is to establish the minimum modeling requirements to capture the effects of submesoscale circulations on the transport of larvae and other material at mesophotic depths in different seasons. Our results show that the connectivity is generally weak and varies significantly depending on the month of the year. In our study area, the transport of material is mainly influenced by the variable shelf currents and by circulation features characterized by spatial scales of the order of 10 km or less.

Key Points:

- The 3D connectivity is low even though the recruitment areas are geographically close to each other, identifying depth as a key isolating factor
- Material dispersion appears to be primarily driven by the extension of shelf currents and the activity of submesoscale structures
- Modeled connectivity in the northern Gulf of Mexico exhibits greater sensitivity to well-resolved sub-mesoscale circulation

Supporting Information:

Supporting Information may be found in the online version of this article.

Correspondence to:

L. Lopera,
lgarcia64@gatech.edu

Citation:

Lopera, L., Bracco, A., & Herrera, S. (2025). Physical connectivity between mesophotic areas in the northern Gulf of Mexico. *Journal of Geophysical Research: Oceans*, *130*, e2024JC021753. https://doi.org/10.1029/2024JC021753

Received 23 AUG 2024
Accepted 27 JAN 2025

Author Contributions:

Conceptualization: Luisa Lopera, Annalisa Bracco, Santiago Herrera
Formal analysis: Luisa Lopera
Funding acquisition: Annalisa Bracco, Santiago Herrera
Methodology: Luisa Lopera
Software: Luisa Lopera
Writing – original draft: Luisa Lopera
Writing – review & editing: Luisa Lopera, Annalisa Bracco, Santiago Herrera

1. Introduction

Climate change and local threats associated with anthropogenic activities highlight the need for effectively conserving vulnerable coral ecosystems (Freeman et al., 2013; Klein et al., 2010). The design and establishment of marine protected areas (MPAs) are pivotal not only for conserving vulnerable ecosystems but also as a key restoration strategy for marine communities (Sullivan-Stack et al., 2022). For MPAs to be effective, managers need information and tools to evaluate ecosystem connectivity, in addition to threat and recovery potentials (Sheehan et al., 2021; Stephenson et al., 2019). Connectivity is defined as the degree to which two geographically separated ecosystems are linked through the interchange of matter, and it is key to health, biodiversity, recovery, and resilience of marine ecosystems (Balbar & Metaxas, 2019; Green et al., 2013; Viehman et al., 2023). The most effective approach to estimating intraspecific connectivity parameters in marine populations is through population genomics (B. D. Zhang et al., 2020; Zhao et al., 2021). Genetic inferences, however, provide a framework to establish connectivity networks at scales relevant to managing MPAs only when coupled with models of ocean circulation and transport of larval particles (Bracco et al., 2019; Quigley et al., 2022).

Modeling tools are essential for predicting and characterizing connectivity patterns in marine ecosystems (Botsford et al., 2009; Raitsos et al., 2017) but modeled connectivity depends strongly on the resolution used (Saint-Amand et al., 2023). It is crucial to establish the minimum resolution or precision requirements of models to accurately represent the physical variability relevant to marine ecosystem's connectivity (Dauhajre et al., 2019). In this study, we explore this problem, testing both time and space resolutions needed to determine the potential connectivity among mesophotic coral habitats in different depth zones in the northern Gulf of Mexico (GoM).

The coastal GoM is one of the world's large marine ecosystems (LME) encompassing the neritic zone and is characterized by elevated productivity and biological diversity, and distinctive hydrography (Gil-Agudelo et al., 2020; Sherman & Alexander, 1986; Turner & Rabalais, 2018). Corals are particularly abundant in this LME, providing essential habitat for many fisheries (Spies et al., 2016). These fisheries, in turn, offer valuable economic and ecological services to both the United States and Mexico. Coral reefs in the GoM also provide shoreline protection from erosion, hurricanes, and tropical storms (Gil-Agudelo et al., 2020). However, despite the crucial ecosystem and economic services provided by corals in the GoM, and the mounting threats to their survival (Dee et al., 2019; Lawman et al., 2022), our understanding of their distribution, diversity, and connectivity remains limited, particularly for the mesophotic and deep-sea populations (Rocha et al., 2018; Studivan & Voss, 2018).

The substrates at the Flower Garden Banks west of the Mississippi Delta and the Pinnacles Trend to the east are among the most extensive known mesophotic coral habitats in the northern GoM (see Figure 1) (Gittings et al., 1992; Locker et al., 2010; Rezak et al., 1983). These habitats host large coral ecosystems and commercially important fish species, including red, gray, and vermilion snapper, black sea bass, scamp, gag, and red porgy (Cairns & Bayer, 2009; Denton et al., 2011; Rezak et al., 1983). They are part of approximately 178,000 km^2 of substrate with the potential to support mesophotic ecosystems in the basin (Silva et al., 2016).

It has been hypothesized that in a warmer ocean, mesophotic coral ecosystems (MCEs) may serve as refugia and reproductive sources to degraded shallower populations, potentially contributing to their long-term resilience (Garavelli et al., 2018; Studivan & Voss, 2018). While this “deep reef refugia hypothesis” has been disputed on the basis of limited overlap in species and connectivity between shallow and mesophotic reefs (Rocha et al., 2018), the renewed interest has brought attention to the many anthropogenic stressors that deeper ecosystems are facing, from overfishing and mining to increasing sedimentation rates. The recognition that MCEs are threatened has further emphasized the need to include them in marine planning worldwide (de Oliveira Soares et al., 2020).

Here, we focus on connectivity between the areas of the Flower Garden Banks National Marine Sanctuary (FGBNMS) and the Pinnacles Trend (Figure 1) (The Florida Middle Grounds was excluded as its coral reefs are found at shallower depths than at the other two sites (Locker et al., 2010) while the Pulley Ridge reefs lie further to the south, close to the eastern and southern boundaries of our model domain). The FGBNMS is a national marine sanctuary protected by the National Oceanic and Atmospheric Administration (NOAA) since 1992 and is located about 180 km offshore the coasts of Texas and Louisiana. The Pinnacles Trend, on the other hand, is located to the east of the Mississippi Delta, extending eastward offshore of the Mississippi Delta toward the Florida shelf. The Pinnacles area is an important recreational and commercial fishing destination with many carbonate mounds with variable levels of relief spread across a broad area. The area is highly biodiverse, featuring azooxanthellate octocorals, sponges, black corals, and stony corals, but is notably lacking in reef-building corals (Silva et al., 2016).

The objectives of this work are to broadly characterize the physical connectivity potential between the areas of the FGBNMS and the Pinnacles Trend while exploring model requirements to better quantify connectivity at mesophotic depths in the northern GoM. This work does not focus on specific coral populations or species as prior studies have (e.g., Garavelli et al., 2018; Liu, Bracco, Quattrini, et al., 2021). Rather, we examine general connectivity patterns and their variability.

Several modeling studies (Barkan et al., 2017; Bracco et al., 2016; Haza et al., 2016; Sun et al., 2020) and observations (D’Asaro et al., 2020; Poje et al., 2014) in the past decade have identified submesoscale circulations (SCs) as fundamental to the dynamics in the region of interest. SCs commonly form near both surface and bottom boundary layers, spanning spatial scales from hundreds of meters to a few kilometers (McWilliams, 2016). Submesoscale circulations, in the form of km-scale vortices, filaments, and fronts, typically exhibit life cycles of

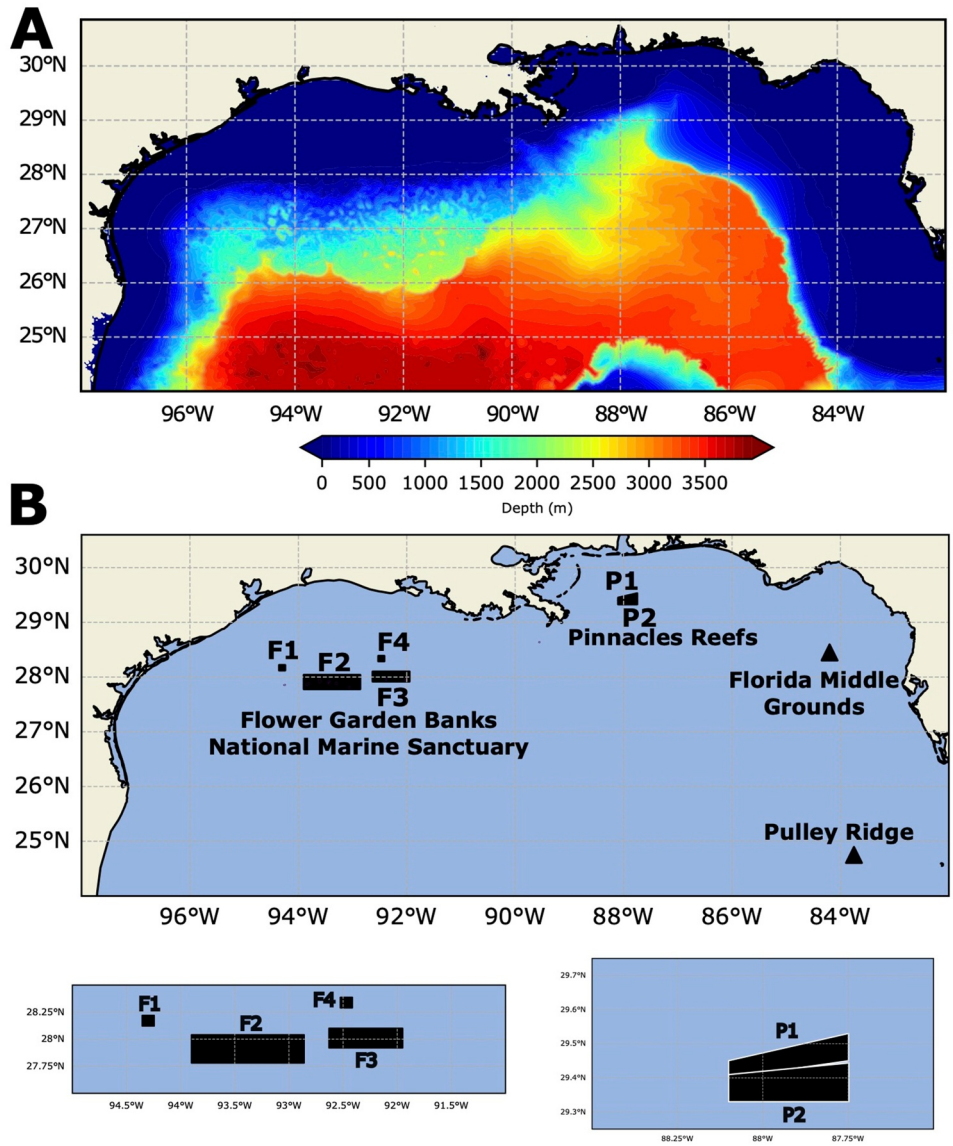

Figure 1. (a) Bathymetry map of the model domain. (b) Location of the mesophotic coral ecosystems in the Gulf of Mexico, with release and receiving areas in the Flower Garden Banks National Marine Sanctuary (F1 to F4, or F zones) and Pinnacles Trend (P1 and P2, or P zones) regions.

hours to a few days and are characterized by Rossby and Richardson numbers of order 1 (Dauhajre et al., 2019; Liu, Bracco, & Sitar, 2021; Sun et al., 2020). They also exhibit seasonal variability, being more prominent during the winter, especially in the form of eddies, when the mixed layer is deeper than the summer season, when, at least in the GoM, fronts are prevalent (Luo et al., 2016; Z. Zhang et al., 2021). Submesoscale circulations can modulate connectivity at time scales from hours to days near the ocean bottom (Romero et al., 2013; Uchiyama et al., 2014), by modifying vertical mixing and contributing to the trapping of material and to its transport along the bottom boundary layer (Bracco et al., 2016, 2018; Cardona & Bracco, 2016; Liu, Bracco, Quattrini, et al., 2021; Saint-Amand et al., 2023; Uchiyama et al., 2014). Given the diurnal variability and the ephemeral characteristics of SCs, recent studies emphasized the need for high-resolution submesoscale-permitting models to accurately represent the impact of submesoscale structures on connectivity metrics (Dauhajre et al., 2019; Liu, Bracco, Quattrini, et al., 2021; Saint-Amand et al., 2023; Sun et al., 2020). However, these models can only be validated in their ability to represent mesoscale circulation and the statistical properties of the velocity field when in situ observations are available. Regional data-assimilative models, indeed, are limited in their ability to be validated with

respect to the SCs by a lack of continuous observations. Only their mean statistics can be compared in some locations, and generally these comparisons are limited to surface quantities (D'Asaro et al., 2020; Poje et al., 2014). This is because currently available satellite data are unable to capture the SCs.

Here, we explore the spatiotemporal impact of SCs, using a realistic submesoscale-permitting regional ocean model run at 1-km horizontal resolution, and we investigate the sensitivity of the resulting connectivity metrics to both temporal and spatial averaging. In our study, we build upon results relevant to the GoM (Liu, Bracco, Quattrini, et al., 2021) and more recently to the Whitsundays, offshore Australia (Saint-Amand et al., 2023), and acknowledge from the start the need for high-resolution (at least 1 km in the horizontal) models. This work is novel in the exploration of the time dimension and downscaling model outputs from submesoscale-permitting model runs for general connectivity studies.

In sum, in this work, we address the following questions:

1. How does potential connectivity between mesophotic reefs in the northern GoM vary over time in relation to its physical drivers?
2. To what extent does the frequency and resolution of submesoscale variability impact the modeled connectivity?

2. Materials and Methods

2.1. Ocean Model Configuration

The model of choice for this work was the Coastal and Regional Ocean COmmunity (CROCO) model (CROCO) in its hydrostatic version. CROCO is a modeling platform based upon ROMS AGRIF and uses a split-explicit time integration (Auclair et al., 2019). The computational grid extends from 24°N to 31°N and from 98°W to 82°W, with open boundaries at the east and south sides (see Figure 1). The resolution is 1 km in the horizontal, with 50 terrain-following levels in the vertical, and an increased bottom stretching parameter, given that we are interested in capturing mixing processes near the seabed. This configuration has been used also to investigate the dispersal patterns of red snapper larvae (Zhou et al., 2024). Except for its vertical discretization, the overall setup follows that in Sun et al. (2022) and its representation of the circulation in the portion of the domain of interest to this work (north of 27°N) is nearly identical in a statistical sense. The grid was built using the 2-min Gridded Global Relief Data (ETOPO2) topography, and a Shapiro smoother of 0.25 was applied to avoid pressure gradient errors (NOAA National Centers for Environmental Information, 2006). CROCO was forced every 3 hours through wind stresses, heat, and water fluxes data obtained from the Navy Global Environmental Model. The freshwater discharge of the 10 most important rivers in the GoM was represented as an additional precipitation flux around the river mouths using daily records from the United States Geological Survey, following Barkan et al. (2017) and Sun et al. (2022).

The south and east boundaries were nudged every 3 hours to the Hybrid Coordinate Ocean Model-Navy Coupled Ocean Data Assimilation (HYCOM-NCODA) analysis system (Cummings, 2006; Cummings & Smedstad, 2013). The initial conditions were extracted from the HYCOM-NCODA database on 1 April 2014, and the first five months of the simulation were discarded as spin-up. The M2, S2, N2, K2, K1, O1, P1, Q1, Mf, and Mm tidal components from the TPXO-7 global tidal model have been also included (Egbert & Erofeeva, 2002).

CROCO was run from 1 September 2014 to 31 August 2016, saving the velocity fields as 30-minute averages for subsequent Lagrangian simulations. Over this period, different configurations in the surface circulation of the region were identified. They include the extension and contraction of the Loop Current (LC), the presence of mesoscale eddies with diameters ranging from tens to hundreds of kilometers, and the eastward current that flows near the shelf edge following the 200-m isobath. Figure 2 provides examples of the circulation patterns just mentioned. A similar configuration to the one adopted here has been validated in previous works (Liu, Bracco, Quattrini, et al., 2021; Liu, Bracco, & Sitar, 2021; Sun et al., 2022). In the Supp. Material, readers can find additional validation of the model outcomes, complementing the results presented in the cited references. The validation includes both surface (Figures S1 and S2 in Supporting Information S1) and near-bottom currents (Figures S3 and S4 in Supporting Information S1), temperature profiles (Figure S5 in Supporting Information S1), and inertial motions at the ocean surface (Figure S6 in Supporting Information S1).

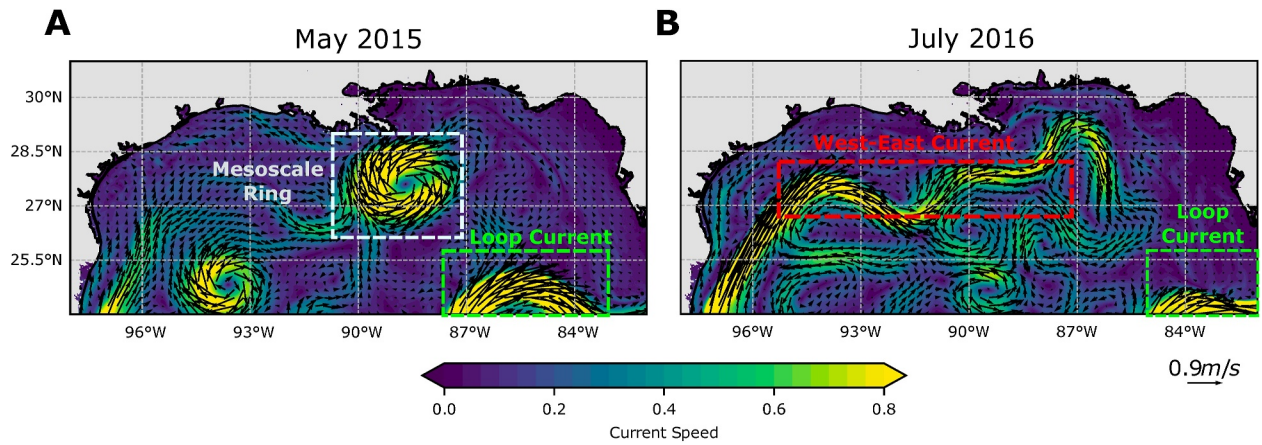

Figure 2. Mean surface currents simulated by the Coastal and Regional Ocean COmmunity model during (a) May 2015 and (b) July 2016 showing the Loop Current, the eastward current near the 200 m isobath (panel B), and a Ring (panel A).

2.2. Lagrangian Particle Dispersion Model

The Lagrangian model Icthyop, version 3.3.12, was used to simulate vertical and horizontal advection of neutrally buoyant particles from September 2014 to August 2016 (Lett et al., 2008). Neutrally buoyant particles were chosen because available observations for mesophotic coral species, while few, concur in their larvae having neutral or even slightly negative bouyancies from the first hours after fertilization up to their PLD. This is the case, for example, of *Swifia*, *Thesea*, and *Muricea* in the GoM (J. Johnstone, personal communication, 19 November 2024) and more generally for *Porites cf. P. lobata* and *Porites compressa*, according to measurements collected in Palau and Hawaii, respectively (Bennett et al., 2024; Rodrigues & Padilla-Gamiño, 2022).

We explored connectivity between mesophotic areas in the northern GoM throughout the year. This choice was dictated by the fact that while mass spawning in shallow corals species in the GoM typically occurs during the summer (June, July, and August), the spawning season for most mesophotic corals and benthic communities remains unknown. A temporal shift in their spawning, compared to surface species, might be anticipated. For instance, Montastraea cavernosa has been identified to spawn from June through November, while *Orbicella faveolata* and *Orbicella anularis* spawn from August to November (Jordan, 2018).

The mesophotic areas around FGBNMS were divided into four zones or areas, F1 to F4, each covering different depth ranges. Additionally, our analysis included two zones, P1 and P2, encompassing the Pinnacles Trend situated to the east of the Mississippi Delta. Figure 1 shows the geographical locations of these areas. The release and recruitment polygons include the following MCEs: F1 includes Stetson Bank, F2, West Flower Garden, East Flower Garden, MacNeil, Rankin, Fathom, Bright, Geyer, and Elvers Banks, F3, McGrail, Bouma, Rezak, Sidner, Parker, and Alderdice Banks, and F4, Sonnier Bank.

In each deployment, the particles were consistently released 0.5 m above the model bottom.

In both F1 and F4, 490,000 neutrally buoyant particles were released at depths ranging from 50 to 60 m. In contrast, 475,000 and 462,303 were released, respectively, at depths ranging between 50 and 160 m in F2, and from 70 to 150 m in F3. For P1, a total of 401,000 particles were released at depths ranging from 45 to 70 m, while in P2, 408,000 particles were released at depths between 70 and 100 m.

Despite the different sizes of the polygons, a similar number of particles, comprised between 401,000 and 475,000, were released in each area, regardless of its total area. As a result, larger polygons have lower particle density and vice versa. However, by releasing a large number of particles in each case and considering a high number of releases (72 per zone), we insured that the connectivity percentages presented in the results are robust in all cases and are not impacted by the density differences at release.

The releases were done on the first, third, and fifth of each month in the two years considered, and particles were tracked for a 30-day period. In this study, we did not replicate specific coral species; thereby, we did not include behavioral models that account for traits such as diel vertical migration or mortality. Instead, our analysis focuses

on the impact of high-resolution 3D fields on neutrally buoyant particle transport to assess connectivity potential at mesophotic depths.

2.3. Sensitivity Simulations

The role of SCs on connectivity has been emphasized in several recent publications. Results from simulations at different resolutions suggest that the contributions of circulations at km scale may vary with the area of interest and depths considered. In the specific case of the GoM, previous works have shown that mesoscale-resolving simulations (with a horizontal resolution of 5–10 km) cannot fully capture the intensity and especially the variability of the velocity field or vertical diffusivity, either at the surface or in the bottom boundary layer (Liu, Bracco, Quattrini, et al., 2021; Liu, Bracco, & Sitar, 2021).

Most importantly, key dynamical quantities continue to differ when the submesoscale-permitting model output is averaged at mesoscale-resolving scales (e.g., Figure 13 in Sun et al., 2020). Here, we assumed that connectivity would differ with a lower-resolution circulation model, and posed the question of how altering the spatial and temporal frequencies of velocity field information from a submesoscale-permitting circulation model might impact connectivity. Averaging the circulation model output over longer time scales or larger spatial scales could save computing time and data storage space, thereby making easier to manage the computational requirements for connectivity studies at scales where SCs are relevant.

Given the major differences in connectivity and circulation between winter and summer months attributed to the seasonality in mixed layer depth and SCs (Luo et al., 2016), we conducted sensitivity tests for January and July 2015. In these tests, we either completely or partially inhibited the diurnal variability of the SCs by advecting particles with Ichthyop using the CROCO velocity field averaged at frequencies of 6 hr, 12 hr, and 24 hr, respectively. The time averaging also contributes to smoothing out the smallest and more ephemeral circulations, usually in the form of submesoscale fronts.

Lastly, we spatially averaged our CROCO outputs on a 5 × 5 km grid and repeated the lower frequency calculations, referred to as 12 hr + Avg and 24 hr + Avg hereafter. The spatial upscaling was also performed by applying a 5-km Gaussian filter, with nearly identical results (not shown).

In addition, for some of those cases, we assessed also if a simple random walk could be used to parameterize the information loss when averaging, using an average vertical diffusivity of $K_z = 10^{-3}$ m^2/s. Submesoscale circulations have limited impacts on overall lateral transport properties but significantly alter vertical transport, amplifying it (Zhong & Bracco, 2013). Using the value of diapycnal diffusivity found in submesoscale-permitting simulations of the GoM at the base of the mixed layer in winter (Liu, Bracco, & Sitar, 2021), which broadly matches the depth of the mesophotic corals, we checked if the connectivity in the high-resolution/high-frequency calculation could be recovered by using a simple turbulence parameterization in place of the detailed depiction of submesoscale dynamics.

2.4. Seasonal Variability: Wind Forcing and Submesoscale Circulations

Physical connectivity is modulated by ocean currents, which, particularly in shelf regions, are constrained by bathymetry and wind forcing (Zavala-Hidalgo et al., 2014; Y. Zhang & Hu, 2021). The wind regime in the GoM is part of the zonal trade system, characterized by strong seasonal variability, which is mirrored by the ocean circulation over the continental shelves (Zavala-Hidalgo et al., 2014). An in depth description of the wind system, its variability and the current response is provided in the Suppl. Material (Figures S7–S9 in Supporting Information S1).

The connectivity analysis conducted in this work was performed monthly; however, a seasonal aggregation was carried out based on wind forcing climatology (Figure 3), accounting for both speed and direction, and consequently, ocean currents climatology. The seasonal classification adopted is as follows: from November to January (winter), when winds are preferentially northeasterlies and strongest in November; from February to April (spring), when winds transition to southeasterlies; from May to August (summer), characterized by highly variable southwesterlies; and finally, September and October (fall), when the winds transition back to northeasterlies.

SCs also follow a seasonal cycling. They are more abundant in winter, when the mixed layer depth is deeper, with a prevalence of submesoscale eddies (Figure 4a). In summer, instead, frontal structures dominate (Figure 4b),

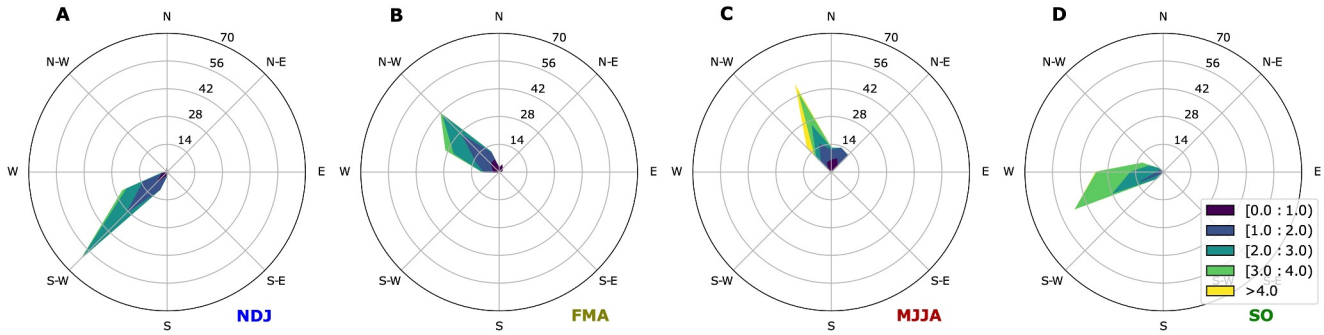

Figure 3. Climatological wind roses for (a) NDJ, (b) FMA, (c) MJJA, and (d) SO calculated using daily data from the Navy Global Environmental Model with an effective resolution of about 0.28° over the available period from 2013 to 2022.

with the freshwater input from the Mississippi River system fueling the density gradients required for the fronts' generation (Luo et al., 2016).

Near the bottom, the submesoscale activity is less sensitive to the season considered but slightly stronger in winter (Figure 4c) than summer (Figure 4d) at the depths of interest, and enhanced over bathymetric features.

Taken together, the wind and submesoscale variability justifies our focus on the winter and summer seasons in the sensitivity analysis.

2.5. Intraseasonal to Interannual Variability: The Loop Current System

Beside the changes in the wind forcing, the upper current system of the GoM is dominated by the presence of the clockwise LC, which brings warm and salty water from the Caribbean Sea through the Yucatan Channel and eventually reaches the Atlantic Ocean via the Florida Strait. The LC extends from the surface to 1,000–1,200 m (Amon et al., 2023; Cardona & Bracco, 2016) and can be found in its contracted state in the south of the basin or extended toward the north, reaching the continental slope (Cardona & Bracco, 2016; Liu, Falasca, &

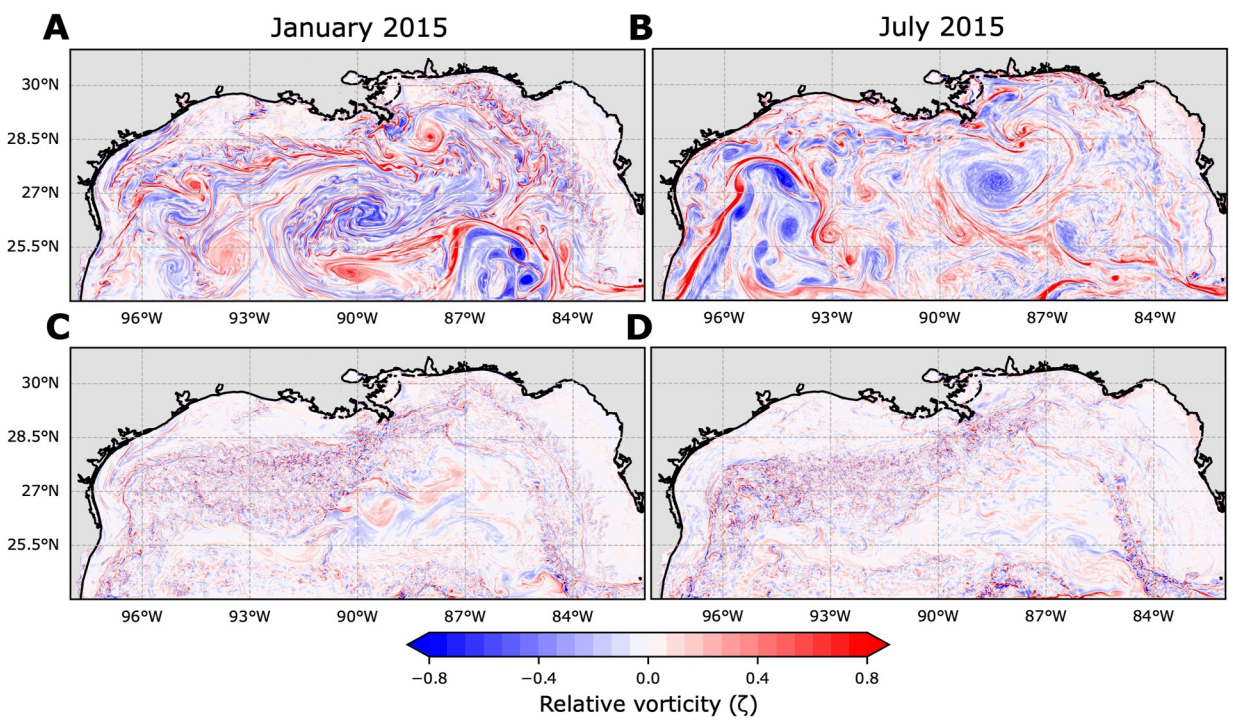

Figure 4. Instantaneous near-surface (top) and bottom (bottom) relative vorticity fields during January (a and c) and July 2015 (b and d).

Bracco, 2021; Sanvicente-Añorve et al., 2018). The LC may influence the circulation around the areas of interest only in its fully extended position but never reaches any of the sites, being constrained by its depth to occupy only areas deeper than 800–1,000 m (see Figure 2).

Large anticyclonic eddies, also known as Rings, with diameters ranging from 200 to 400 km, detach from the LC at irregular intervals (from 2 to 18 months), and then exhibit average propagating speeds of 2–5 km per day (Amon et al., 2023; Cardona & Bracco, 2016; Cardona et al., 2016; Zhu & Liang, 2022). Rings typically travel westward, interacting with the complex bathymetry and loosing strength (Cardona & Bracco, 2016; Cardona et al., 2016; Zeng et al., 2015). In the northwestern GoM, the mean flow along the continental slope is primarily influenced by the extension of a western boundary current that flows eastward, while the continental shelf offshore of Texas and Louisiana is characterized by weak and highly variable flow patterns primarily driven by wind stress that varies at seasonal scales (Garavelli et al., 2018; Sanvicente-Añorve et al., 2018).

We selected the period from late 2014 to 2016 due to the markedly different conditions that were observed during this timeframe. Despite lacking any data assimilation, CROCO captures well the significant differences observed in the LC position during the years under consideration (Figures 2a and 2b, and Figures S1–S2 in Supporting Information S1).

Between September 2014 and August 2015, the LC, in an extended position, occupied the northern GoM reaching as far north as 26°N, and the shelf current was only sporadically discernible. In contrast, during late 2015 and 2016, conditions were closer to the climatological patterns, with small (tens of km) and short-living mesoscale eddies at the latitudes of interest, and the LC extending no further than 25°N. The continental shelf current was more active in 2016, with its maximum strength simulated during the summer season (see Figure 2).

2.6. Connectivity Matrixes and Quantifications

In this study, two sites display three-dimensional (3D) connectivity potential when the following criteria are met:

1. A particle released in one of the zones illustrated in Figure 1b is detected in any other zone within a 30-day period.
2. The particle is found within a depth range of ±15 m relative to the bottom of the receiving site.

In contrast, two-dimensional (2D) connectivity neglects the depth threshold.

In our calculations, a single particle can be counted multiple times if it reaches different polygons over its month-long life, to best evaluate the potential for long-distance connectivity across sites. The percentage of particles successfully exchanged between two sites is then visualized using connectivity matrices with the source sites located along the vertical axis and the sink sites along the horizontal one. The zones are arranged in the matrix based on their longitudinal position, from west to east. Each *i*–*j* connection in the matrix represents the percentage of particles released in location *i* that successfully reached location *j*. Links above the diagonal indicate west-east connectivity, whereas those below the diagonal suggest east-west connectivity.

3. Results

3.1. Regional Horizontal Dispersion

The direction of particle motion and the horizontal traveled distances exhibit seasonal and intra-seasonal variations. As previously mentioned, the shelf circulation in the GoM is primarily wind-driven and seasonally variable, especially in the central portion of our domain. For example, wind variability during November 2014 can be seen in Figure S9 in Supporting Information S1. Even though the wind direction is predominantly to the south, there are weather events with winds blowing in all directions reaching speeds up to 12 m/s. This variability in the momentum forcing is imprinted in the surface dynamics as quantified by the high standard deviations of zonal and meridional velocities near the areas of the FGBNMS and the Pinnacles Trend (see Figure S8 in Supporting Information S1).

Figure 5 illustrates the total monthly average area covered by the particles after 30 days of transport. Such area is quantified based on the model grid, which has a 1 km × 1 km horizontal resolution. For each particle, we identified the nearest 1 km^2 pixel 30 days after its release, and then summed the total number of pixels containing particles.

Within the FGBNMS, the area starts to increase in October, peaking at approximately 100,000 km^2 in winter (January), independently of the year. Subsequently, the area covered diminishes, dropping to less than 10,000 km^2

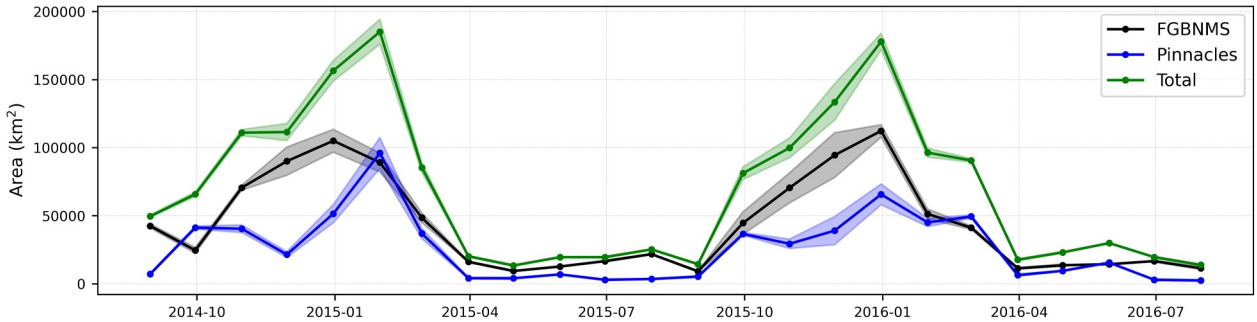

Figure 5. Time series of the area covered by the particles after 30 days of transport for each month considered.

during the summer season. Similarly, in the Pinnacles Trend, the largest area was recorded in February 2015, approaching 95,000 km^2, and the smallest in August 2016, with about 2,500 km^2. Despite the significant differences in mesoscale circulation in the GoM in the two years considered, the area covered remains comparable, with a strong seasonality and larger interannual differences at the Pinnacles than the FGBNMS.

Even though the average area in Figure 5 shows a clear seasonal pattern, the direction and the distance traveled by the particles are highly variable at intraseasonal scales. For instance, Figure 6 illustrates the 3-dimensional position of the particles after 30 days of transport during September (A) and October (B) 2014. Even within the same climatological season, dispersal patterns exhibit significant differences. In September, particles in FGBNMS dispersed westward along the 200-m isobath and southward, extending as far as 26°N. In contrast, during October, the transport is predominantly meridional (i.e., north-south). Regarding the area of the Pinnacles Trend, the particles remain within isobaths in September with slight movements toward the northeast and southwest. Conversely, in October, there is an important displacement to the southwest, with particles approaching the area of the FGBNMS, and a slight southward transport indicated by the green arrows.

3.2. Modeled Potential Connectivity

The seasonal ensemble of simulated connectivity from September 2014 to August 2016 in the northern GoM is summarized in Figure 7. First, three-dimensional connectivity at mesophotic depths is found year-round and is characterized by substantial variability with no apparent seasonal dependency in the direction of connectivity (connections above and below the diagonal as indicated by the black arrows in Figure 7). Despite the lack of definitive seasonal patterns, higher connectivity occurs in winter (NDJ) and spring (FMA) in both areas. In contrast, fewer connections are observed during summer, with fall providing intermediate values.

Second, the most robust and consistent interchange of material year-round takes place between P1 and P2 regardless of the season and year (blue arrows). The 3D connectivity between P1 and P2 ranges between 21% and 35%, reaching its maximum during the winter (NDJ). In contrast, for the FGBNMS areas, the potential connectivity is usually below 5% (yellow arrows in Figure 7). This holds true despite the relatively small geographical distances between zones, ranging between 20 and 180 km.

Third, the areas of the FGBNMS and the Pinnacles Trend are largely isolated from each other, as no connections were identified in the ensemble mean where connectivity below 0.25% were considered null (highlighted by red rectangles in Figure 7). However, rare episodes of long-distance connectivity do occur. For example, P1 particles

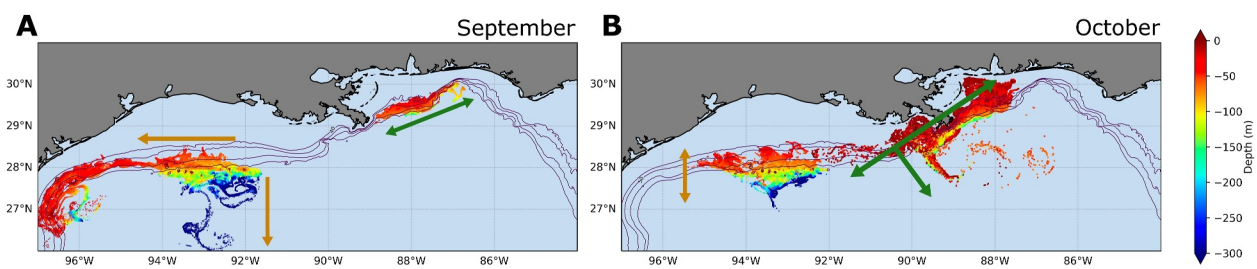

Figure 6. 3D position of the particles after 30 days of transport during (a) September and (b) October 2014. Arrows illustrate the main directions of transport.

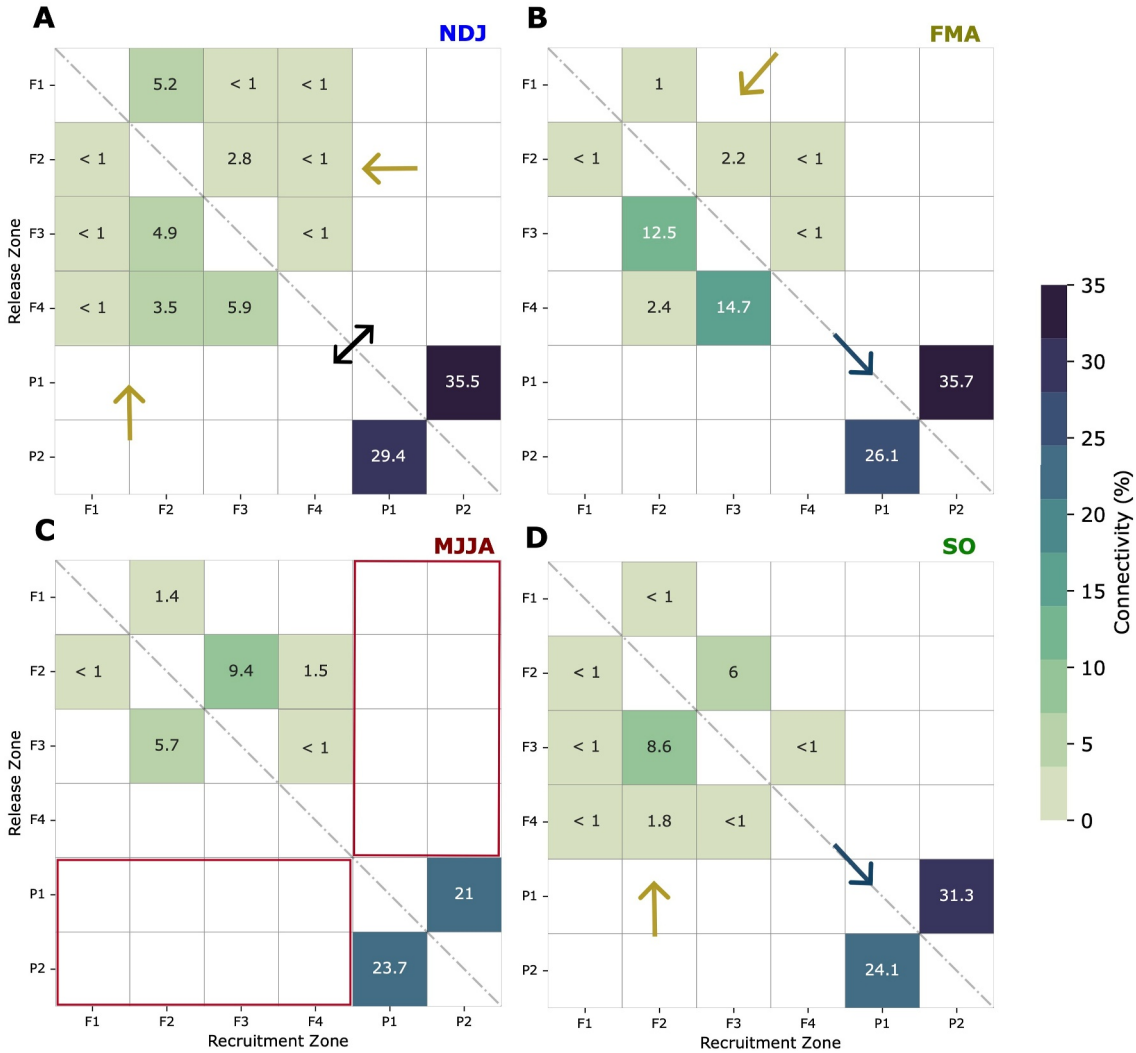

Figure 7. Seasonal ensemble mean 3D connectivity matrixes for (a) Winter NDJ, (b) Spring FMA, (c) Summer MJJA, and (d) Fall SO. Black arrows highlight the existence of connections above and below the diagonal, blue arrows point to the robust and consistent interchange of material between P1 and P2, yellow arrows point to the weak strength in connections within Flower Garden Banks National Marine Sanctuary, and red boxes highlight the lack of connections between areas.

reached F3 and F4 in October and November 2014 (purple circle in Figure 8b) with probability less than 1%. In February of both years, particles released in the area of the Pinnacles were able to reach Florida Middle Grounds and Pulley Ridge. This episodic connectivity supports the notion of high intraseasonal variability in the basin. In contrast, no particles released in the area of the FGBNMS ever reached the Pinnacles area at the required depth to be considered connected over any 30-day period.

Figure S10 in Supporting Information S1 presents the seasonal ensemble average of connectivity matrices throughout both years of simulation. Winter and spring emerge as the most interconnected seasons, exhibiting the largest number of connections than summer and fall, which are the most isolated, with the fewest connections. Overall, the number of links within years differs by 1 or 2 for all seasons except winter, when 5 more links appeared in 2015 than 2014. In terms of the strength of the connections, there is no evident pattern indicating an increase or decrease during the second year of simulation (less energetic) compared to the first one (more energetic), with at least 80% of the links remaining below the 10% threshold.

Table 1 presents the percentage of particles received and contributed by each area during the 2 years of simulation, calculated based on the total number of released particles. In other words, it shows the relative significance of each zone as a sink and source, respectively. Notably, the smallest and northernmost areas, F1 and F4, were

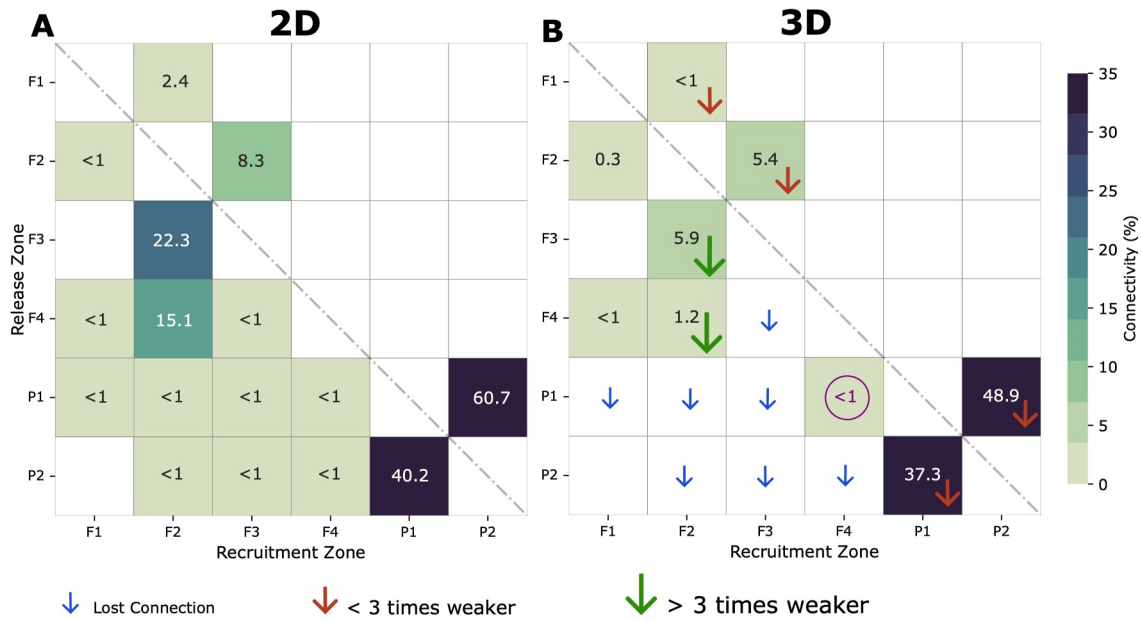

Figure 8. (a) 2D versus (b) 3D connectivity in November 2014. Arrows in panel B indicate significant changes in connectivity when the depth threshold is included compared to the 2D case. Blue arrows indicate lost connections. Red arrows indicate a decrease in connectivity of less than 50%. Green arrows indicate a decrease in connectivity of more than 50%.

identified as the least influential sinks, accounting for 0.05% and 0.2%, respectively. Conversely, P1 and P2 emerged as the most important ones, representing 3.9% and 4.7%, respectively. F2 and F3 exhibited intermediate values, both close to 2%.

As for sources, F1 was the least influential, with less of 2%, while F4 reached 7.1%. Conversely, P1 and P2 stood out as the largest sources, maintaining consistent percentages above 20%. The high percentages of P1 and P2 as both sources and sinks are attributed to the strong interchange of material between them. In other words, P1 serves as both a source and a sink for P2, and vice versa, but interactions with F areas are very limited. F2 and F3 zones displayed intermediate behavior, contributing 7% and 8%, respectively.

Furthermore, depth was identified as a significant factor limiting connectivity among nearby sites in the FGBNMS area. This is illustrated in Figure 8, which compares 2D and 3D connectivity during November 2014. By including the depth threshold, six connections are lost (indicated by blue arrows in Figure 8b), several others decrease to more than half of the 2D value (green arrows), and, most importantly, episodic connectivity between the two environments (FGBNMS and Pinnacles Reef) is disrupted.

Table 1
Average Percentages of Particles Received (Sink) and Contributed (Source) by Each Zone During the Two Years of Simulation

	Sink (%)	Source (%)
F1	0.05	1.7
F2	2.0	7.0
F3	1.9	8.0
F4	0.2	7.1
P1	3.9	31.0
P2	4.7	25.0

Note. The percentages were calculated based on the total number of released particles.

3.3. Sensitivity Study

3.3.1. Changes in Connectivity

Figures 9 and 10 display connectivity matrices for January and July 2015, respectively. These figures show how the connectivity metrics change when current velocities are averaged over time alone versus when they are averaged over both time and space. In winter (Figure 9), connections do not change significantly across spatial or temporal averaging. The highest temporal resolution case of 30 min exhibited the largest number of successful connections, totaling 11, one of which had a very small probability and was never recovered when using longer time averaging. In each scenario, a minimum of 50% of the successful connections remained below 1% within the FGBNMS area. For the Pinnacles area, the strength of the connection between P1 and P2 exceeded 30% in all cases, reaching up to 80% in the 24 and 12 hr scenarios. Conversely, the strength of the opposite direction, from P2 to P1, peaked at

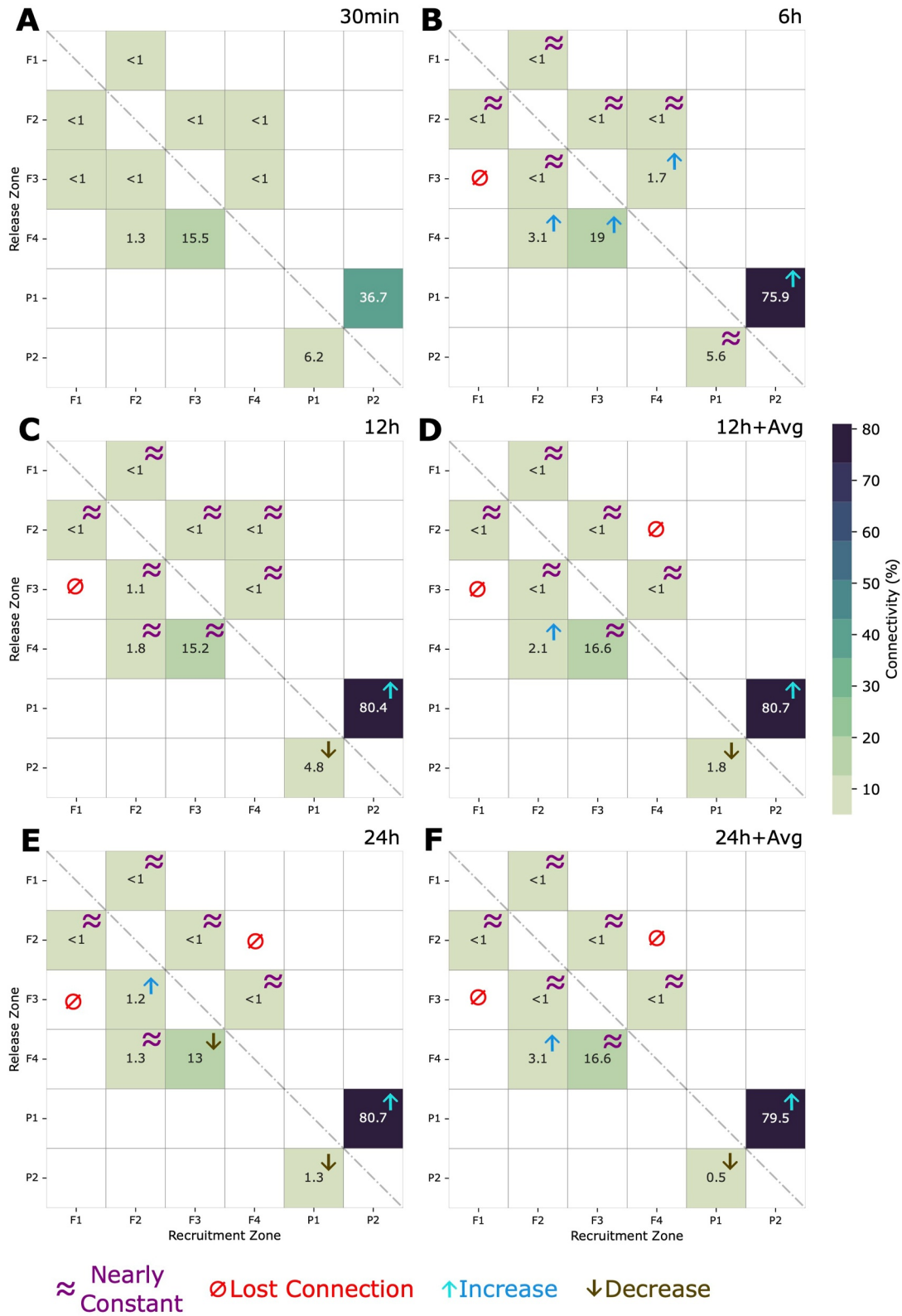

Figure 9. Ensemble connectivity matrices under (a) 30-min, (b) 6-hr, (c) 12-hr, (d) 12-hr + Avg, (e) 24-hr, and (f) 24-hr + Avg forcing scenarios during January 2015.

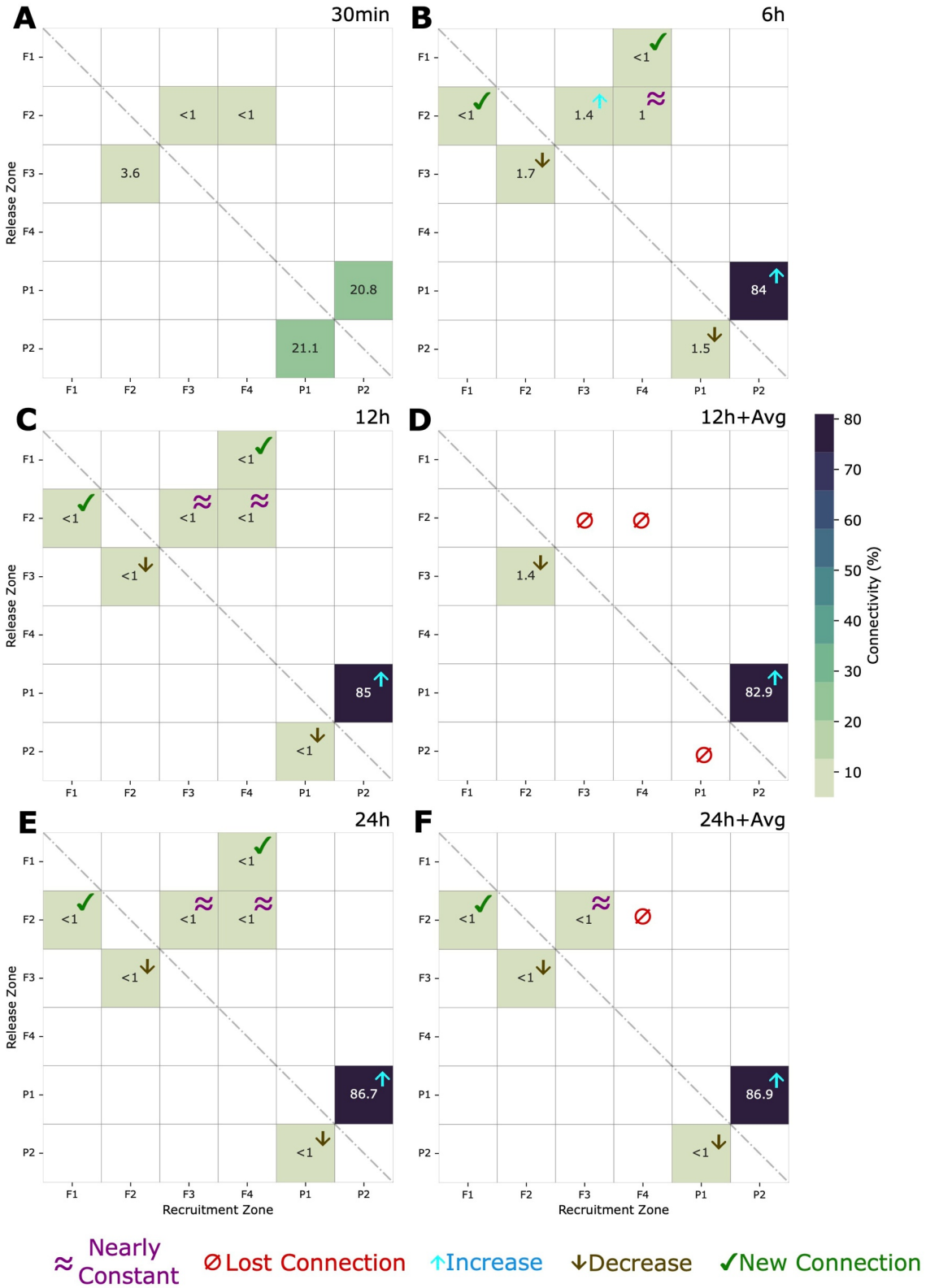

Figure 10. Ensemble connectivity matrices under (a) 30-min, (b) 6-hr, (c) 12-hr, (d) 12-hr + Avg, (e) 24-hr, and (f) 24-hr + Avg forcing scenarios during July 2015.

Table 2
Zonal and Meridional Distances and Standard Deviations for Flower Garden Banks National Marine Sanctuary Areas During January and July 2015

FGBNMS							
January		July		January		July	
Zonal distance (km)				Meridional distance (km)			
30 min		**30 min**		**30 min**		**30 min**	
92 ± 59		83 ± 75		23 ± 17		23 ± 21	
6 h		**6 h**		**6 h**		**6 h**	
85 ± 58		75 ± 70		21 ± 17		22 ± 19	
12 h	**12 h + Avg**	**12 h**	**12 h + Avg**	**12 h**	**12 h + Avg**	**12 h**	**12 h + Avg**
83 ± 58	62 ± 44	71 ± 65	69 ± 66	21 ± 16	15 ± 11	20 ± 17	19 ± 15
24 h	**24 h + Avg**	**24 h**	**24 h + Avg**	**24 h**	**24 h + Avg**	**24 h**	**24 h + Avg**
86 ± 60	80 ± 57	67 ± 68	62 ± 60	19 ± 17	20 ± 17	17 ± 15	17 ± 13

approximately 6% in the 30-min case and reached its minimum at 24 hr with around 1%. Additionally, no significant differences were found when the 5 km × 5 km average was included in the 12- or 24-hr time averages. This behavior at Pinnacles is linked to the role that small and ephemeral vorticity structure plays in transporting material against the mean current direction. When the impact of these structures is averaged out by time-averaging, the mean winter current, which is from P1 to P2, dominates the connectivity.

In summer (Figure 10), the differences are more conspicuous. For example, while 5 links were identified in the 30-min case, the number increased to 7 in the 24-hr, 12-hr, and 6-hr cases, decreased to 2 in the 12-hr + Avg case, and remained the same in the 24-hr + Avg scenario. In the lowest time resolution cases, many links have low probability (below 1%), except for the P1-P2 link, which typically represents the strongest connection. In contrast, in the 6-hr and 30-min forcing scenarios, links above 1% were more predominant, being associated with transport by SCs (fronts predominately) that are averaged out when longer times are considered. The greatest differences between the lower and higher frequency scenarios occurred in the Pinnacles area, where the strength of the connections (P1-P2 and P2-P1) shifted from ∼6% to 37% (30 min) to <1% and to ∼80% (24 hr + Avg), following the preferential direction of the mean circulation in summer.

When changing resolution from submesoscale-permitting to mesoscale-resolving, the horizontal dispersion remains comparable after the first day, but vertical dispersion decreases. In the GoM, previous work quantified such decrease, showing that in a 5-km horizontal resolution the averaged vertical diffusivity is $k_z \sim 10^{-4}$ m^2/s at a depth of about 80–100 m depth, against $k_y \sim 10^{-3}$ m^2/s whenever the lateral model resolution is 1 km (Liu, Bracco, & Sitar, 2021). Assuming that space and/or time-averaging have a comparable impact, we tested if the submesoscale impacts on the vertical transport could be accounted in the lower frequency connectivity calculations by parameterizing vertical dispersion with a random walk scheme with $k_z \sim 10^{-3}$ m^2/s (see Supp. Mat.). The comparison of Figure S11 in Supporting Information S1 with Figures 9 and 10 reveals that the lower-resolution scenarios (24 hr and 24 hr + Avg) remain largely consistent with each other, regardless of whether the random walk scheme is included, both in winter and summer. This suggests that a random walk parameterization is not sufficient to account for the nongeostrophic, small-scale, and short time impacts of the SCs on connectivity.

3.3.2. Changes in Horizontal Distribution

We explore distinct connectivity behaviors in winter and summer, separately examining lateral and vertical transport within the areas of the FGBNMS and the Pinnacles Trend. Tables 2 and 3 provide a summary of the zonal and meridional distances traveled by the particles after 30 days in January and July 2015, encompassing both areas. Overall, longer zonal and meridional distances were observed for the highest frequency scenarios (6 hr and 30 min) in both summer and winter. This indicates that SCs enhance the distance traveled by the particles. Differences, however, tend to increase when spatial averaging is included. Submesoscale frontal systems along the shelves are ephemeral and easily averaged out, especially in summer when they are generally weaker and

Table 3
Zonal and Meridional Distances and Standard Deviations for Pinnacles Trend Areas During January and July 2015

Pinnacles							
January		July		January		July	
Zonal distance (km)				Meridional distance (km)			
30 min		**30 min**		**30 min**		**30 min**	
70 ± 52		46 ± 18		31 ± 42		26 ± 27	
6 h		**6 h**		**6 h**		**6 h**	
81 ± 48		45 ± 18		54 ± 72		20 ± 24	
12 h	**12 h + Avg**	**12 h**	**12 h + Avg**	**12 h**	**12 h + Avg**	**12 h**	**12 h + Avg**
72 ± 46	57 ± 30	35 ± 17	19 ± 12	34 ± 48	24 ± 28	9 ± 13	11 ± 6
24 h	**24 h + Avg**	**24 h**	**24 h + Avg**	**24 h**	**24 h + Avg**	**24 h**	**24 h + Avg**
68 ± 52	54 ± 30	33 ± 17	30 ± 15	25 ± 40	24 ± 33	9 ± 11	7 ± 6

shallower, but they play an important role in modulating connectivity. Those differences are reflected in Figure 11.

In winter, the impact of time-averaging is still clearly visible in the lateral spreading, as submesoscale eddies typically have a lifespan of few days, and overall, the meridional and zonal distances differences are higher than summer.

Figures 12 and 13 depict the 3D positions of particles under all considered scenarios after 30 days of transport during winter and summer, respectively. It is important to note the ability of the higher frequency scenarios to

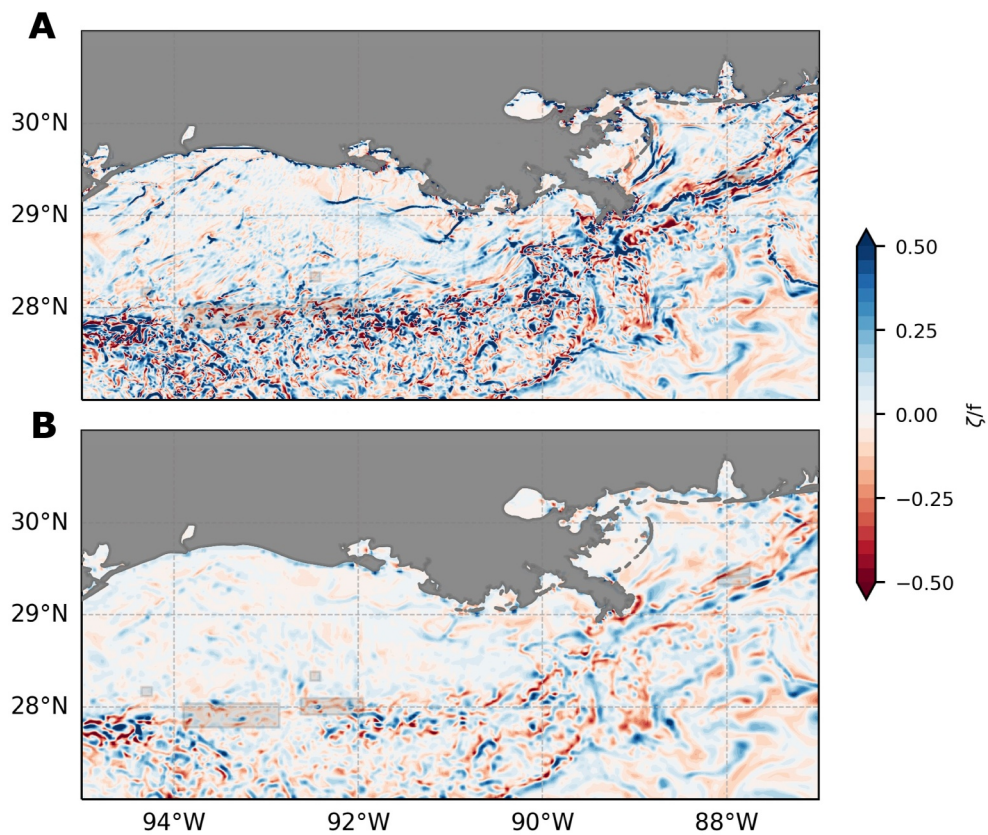

Figure 11. Vorticity fields above bottom on 1 July 2015 for (a) 30-min and (b) 24-hr + Avg scenarios.

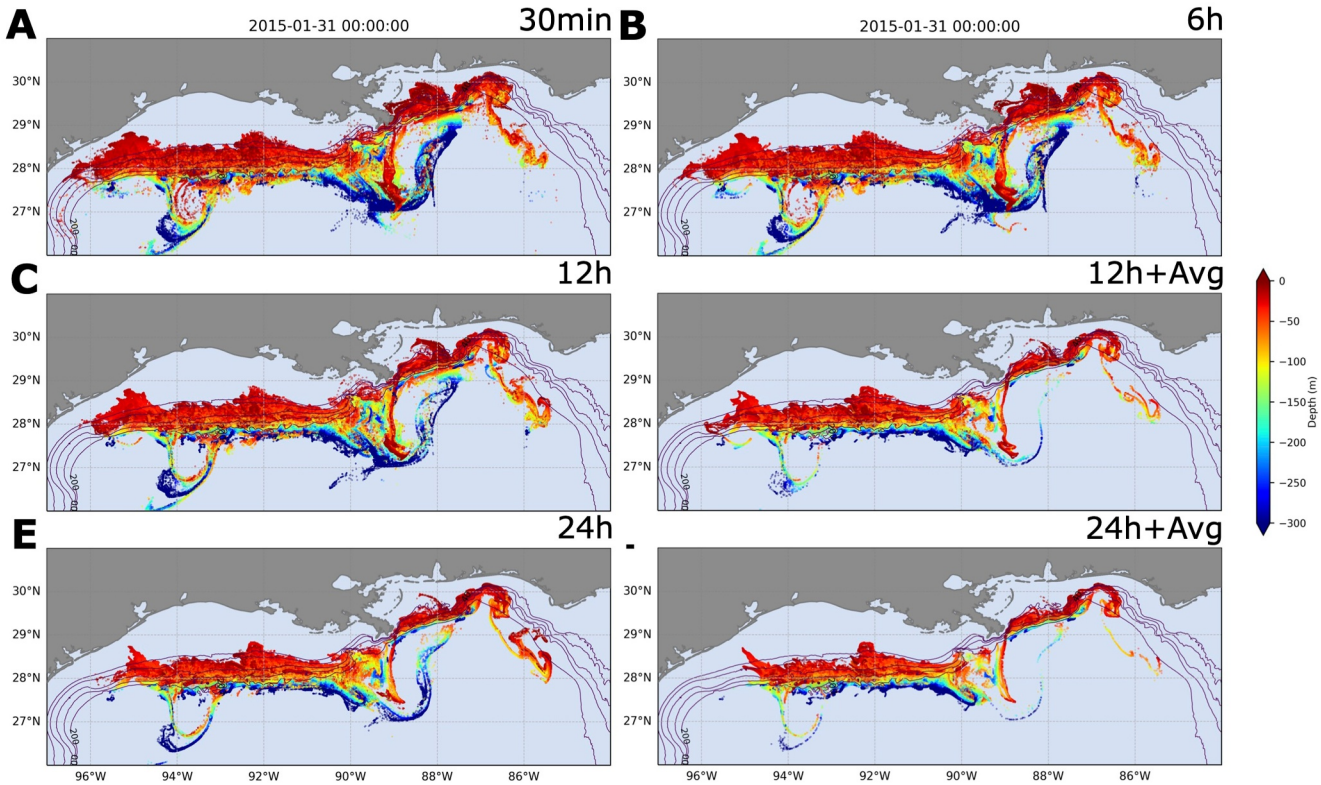

Figure 12. 3D position of the particles after 30 days of transport for (a) 30-min, (b) 6-hr, (c) 12-hr, (d) 12-hr + Avg, (e) 24-hr, and (f) 24-hr + Avg forcing scenarios during January 2015.

spread out more particles over greater distances. This is especially evident during the winter season in both the FGBNMS and the Pinnacles areas (see Figure 12).

The onshore and offshore transport of particles are also significantly influenced by the presence of SCs. Tables S1 and S2 in Supporting Information S1 summarize onshore and offshore transport probabilities for both FGBNMS and the Pinnacles areas during January and July 2015. In both winter and summer seasons, higher frequency scenarios lead to a decrease in the offshore transport of particles in both areas. This effect is more pronounced during the summer season. For instance, in the FGBNMS, offshore transport decreases by 50% from 30-min to 24-hr scenarios, while for the Pinnacles area, it decreases by 83%. In contrast, during winter, there is a decrease of approximately 15% for FGBNMS and 22% for the Pinnacles area.

3.3.3. Changes in Vertical Distribution

Vertical velocities are significantly modified by SCs. Figure 14 illustrates the vertical distribution of all particles after 30 days of transport for both winter and summer, separately for the FGBNMS and Pinnacle areas. As expected, vertical spreading is greater in winter, when the mixed layer is deeper and can reach the release depths, than in July, when it is shallower. This result also aligns with stronger currents during winter, coupled with more pronounced submesoscale features (see Figure 2) that amplify the offshore transport of particles and their subsequent deepening. In the case of the FGBNMS, the mean vertical distribution of particles remains consistent across scenarios, particularly during the winter season. However, more extreme values are observed in the 30-min, 6-hr, and 12-hr scenarios during January, with particles reaching up to 1,700-m depth. Submesoscale frontal and filament systems tend to trap and subsequently deepen the material, and their influence is attenuated when averaging is applied. In July, although the mean depth and the maximum vertical spread remain similar, particles tend to reach greater depths when the currents are averaged over longer periods. These results are supported by the increased offshore transport of particles when SCs are inhibited. For instance, in January, 61% of the sample is transported offshore in the 30-min case, compared to 72% in the 24-hr scenario and 75% in the 24-

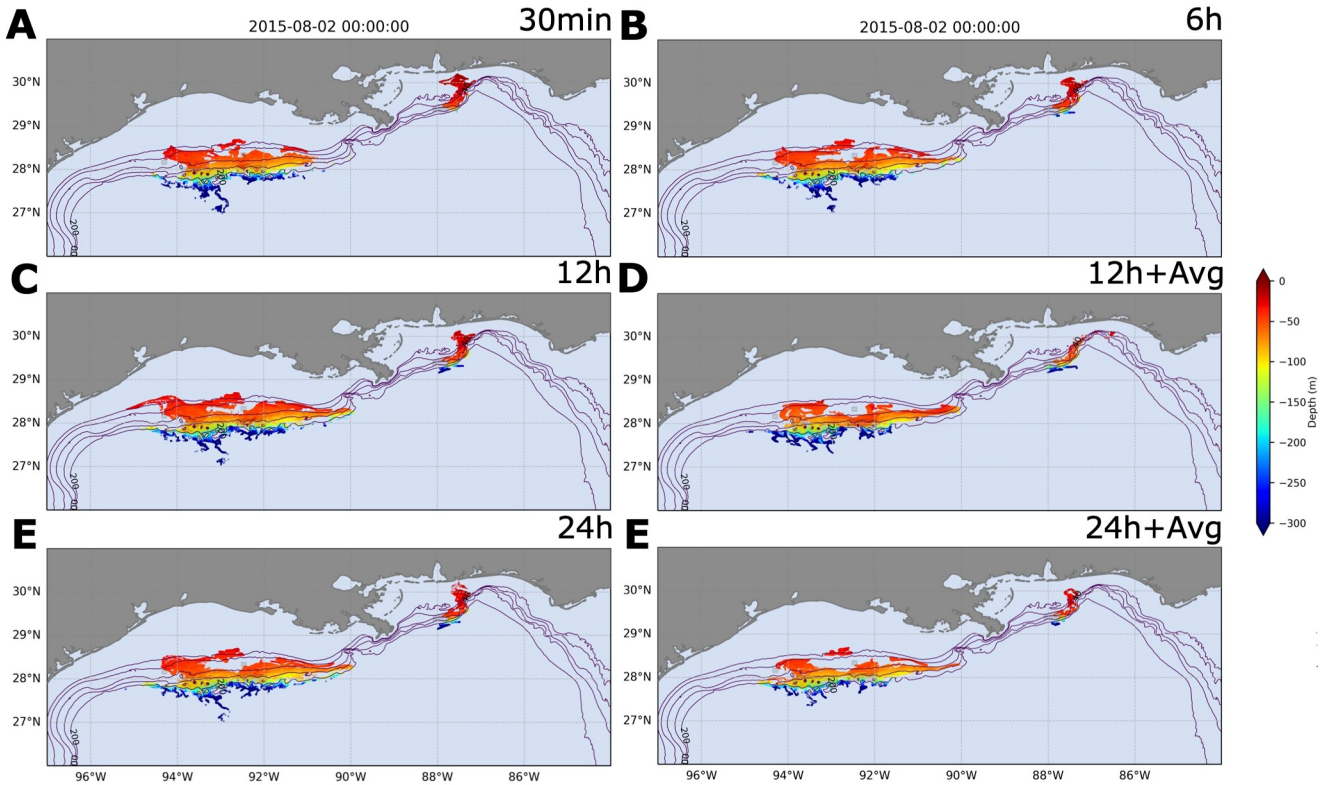

Figure 13. 3D position of the particles after 30 days of transport for (a) 30-min, (b) 6-hr, (c) 12-hr, (d) 12-hr + Avg, (e) 24-hr, and (f) 24-hr + Avg forcing scenarios during July 2015.

hr + Avg. In July, the transport increases from 17% in the 30 min case to 34% and 33% in the 24 and 24 hr + Avg, respectively.

In the case of the Pinnacles area, the similarity in vertical distribution among the highest frequency scenarios persists in both seasons, with a slight decrease in the mean in July. In the remaining cases, the mean position of the particles tends to deepen when the advecting velocity fields are averaged over longer time scales. This is particularly evident when averaged in both space and time. Similar to FGBNMS, vertical distributions in the Pinnacles area tend to deepen when submesoscales are not well resolved, as evidenced by elevated offshore transport in those cases (Tables S1 and S2 in Supporting Information S1). However, this behavior is magnified in P zones when the average in space is also incorporated, potentially highlighting the role of steeper bathymetry.

4. Discussion

The goal of this work was to evaluate the role played by the ocean current in transport and mixing neutrally buoyant material. To do so, we purposefully did not consider any specific biological trait; instead, we focused on the 3D pathways of physical connectivity between mesophotic environments simulating the transport of neutrally buoyant particles. We employed submesoscale-permitting numerical simulations saved at 30-min frequencies and advected a large number of particles offline, releasing them in areas known to be occupied by mesophotic corals.

4.1. Physical Transport Patterns

Focusing first on the highest resolution results (ocean currents resolved at 1 km horizontal resolution and saved as 30-min averages), our findings align with previous studies that investigated physical connectivity at greater depths. Physical transport in the GoM is primarily constrained by the bathymetry, with higher dispersal distances in winter than summer (Bracco et al., 2019; Cardona et al., 2016; Liu, Bracco, Quattrini, et al., 2021). At mesophotic depths, physical transport is found to be notably restricted by the 200-m isobath located around 27.5°N,

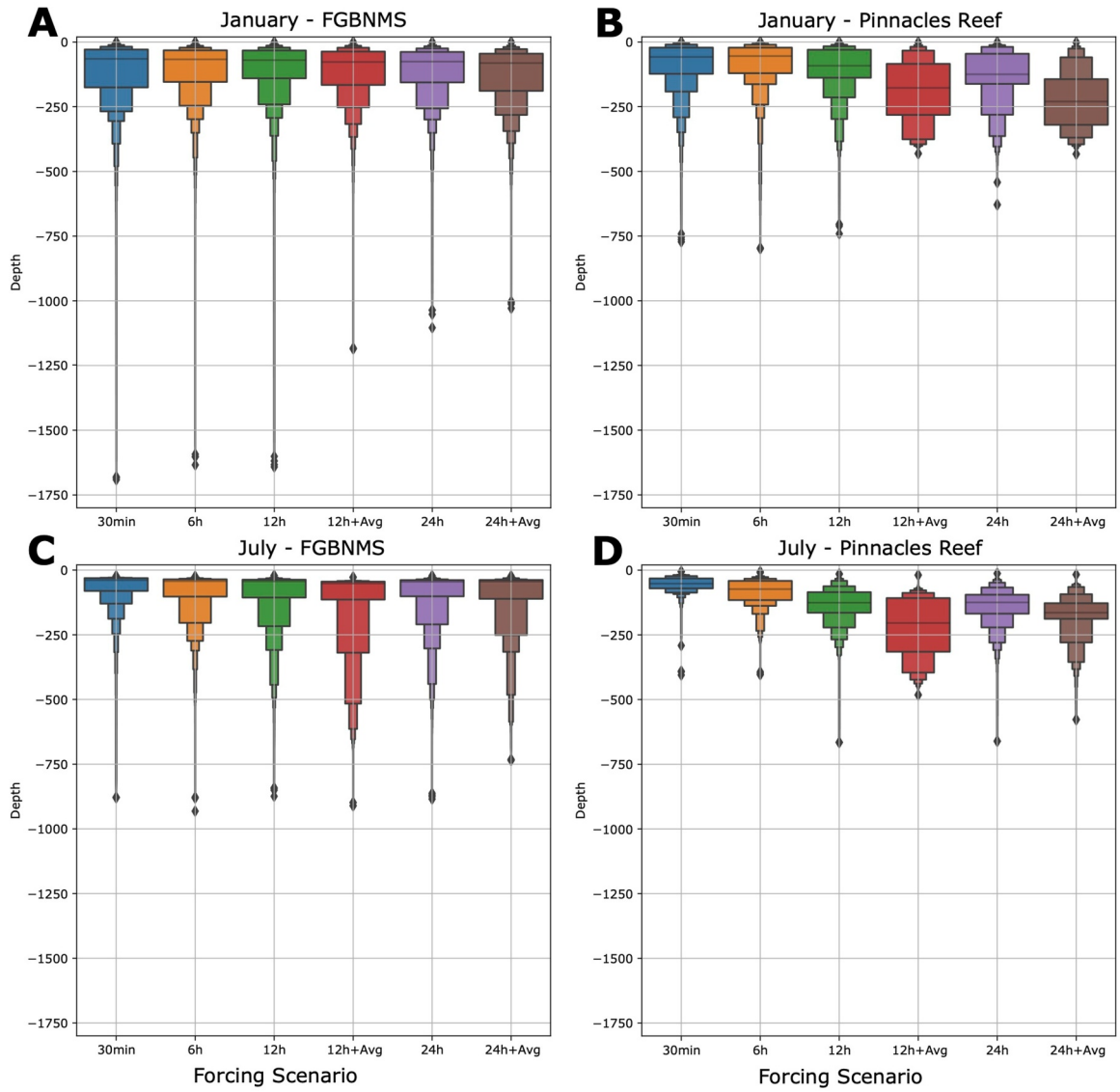

Figure 14. Vertical position of particles after 30 days of transport in January, with (a) and (c) representing the Flower Garden Banks National Marine Sanctuary area and (b) and (d) representing the Pinnacles area.

resulting in most of the simulated pathways being constrained inshore of it (Figure 6). This is especially true during the summer season. Particle dispersion beyond the FGBNMS region increases in September and peaks in the winter months (NDJ). During spring and summer, particles released in the FGBNMS remain mostly within its boundaries, constrained between the 40- and 200-m isobaths. The meridional transport is therefore weak for most of the year, in agreement with Garavelli et al. (2018). Within the Pinnacles area, the highest dispersal potential is observed from October through March (Figure 5). In October, we identified a rare instance of particles that crossed the Mississippi River mouth area and reached the FGBNMS area, while in March, the dispersal patterns suggest potential long-distance connectivity with the Florida Middle Grounds and Pulley Ridge (Figure 8 and Figure S10 in Supporting Information S1). The potential connectivity identified from the Pinnacles area to Florida Middle Grounds/Pulley Ridge supports the notion of mesophotic reefs acting as sources of material for shallower environments, which could enhance their ecological resilience (Łuczyński et al., 2023). Finally, the observed horizontal dispersal patterns may indicate robust connectivity between the FGBNMS area and the shallow-mesophotic coral in the South Texas Banks during September, October, November, and December.

We note that we limited our connectivity study to a 30-day period, and under this constraint, we did not identify any connectivity potential between the FGBNMS and the Florida Middle Grounds/Pulley Ridge as highlighted by Garavelli et al. (2018). However, it would be worthwhile to include longer transport durations to confirm the hypothesis.

Overall, the potential 3D connectivity among the zones identified was weaker, with over 70% of connections remaining below 5% when depth was considered. This was true even for areas geographically close to each other. In contrast, lateral 2D connectivity was notably higher across all cases, supporting the notion that depth acts to isolate areas within the mesophotic band, as it does for the deeper environments (Bracco et al., 2019). Hence, in the design of MPAs, it is imperative to consider that small differences in depth may prevent material exchanges even for close-by sites (Levin et al., 2018; Slattery et al., 2011). Overall, the physical connectivity did not exhibit a preferential direction at the depths considered, because of the highly variable oceanographic conditions at intraseasonal scales. When comparing simulations across years, we observed that although there were large differences in the surface ocean kinetic energy, the position of the LC, and more generally the mesoscale circulation patterns, the overall area occupied by the particles, their mean dispersion distances (Figure 5), and the connectivity among zones did not differ significantly. This is due to the LC being deep (over 1,000 m) and not penetrating into the mesophotic areas. Therefore, near-bottom dispersion in the considered depths is primarily controlled by the extension of the shelf currents and by SCs. These results support the idea of high-frequency circulations as main driver of potential connectivity between remote coral ecosystems (Vogt-Vincent et al., 2023). Lastly, it is worth highlighting that the simulations revealed that only a low percentage of particles was received by zones F1 and F4 in the FGBNMS region (Table 1). These areas are the smallest and northernmost zones and encompass Stetson and Sonnier banks, respectively.

4.2. Modeling Strategy

The second objective of this work was to explore how the representation of potential connectivity related to physical transport changes as a function of the frequency at which the advecting velocity input to the particle transport model is saved. We stress that we designed the sensitivity study by acknowledging that SCs play a crucial role and have to be represented, on the basis of previous results (Dauhajre et al., 2019; Haza et al., 2016; Sun et al., 2020). Our goal was to explore if it was possible to average their impact over time (up to 24 hr) and space (up to 5 × 5 km), and to recover similar potential connectivity metrics observed at higher resolutions.

The sensitivity simulations indicated that potential connectivity is not significantly affected by temporal resolution during the winter season, when mean currents are stronger and the mixed layer extends to the bottom (Figures 12 and 14, and Table 2). In this season, the dominant SCs were eddies generated through baroclinic instability of the mixed layer, which have a radius of few kilometers and last several days. In contrast, during the summer season, when mean currents in the region are weak, the mixed layer depth is shallow (<20 m deep) and the SCs are dominated by frontal structures, a higher number of connections were identified in the 24- and 12-hr average scenarios than the 30-min case (Figures 13 and 14, and Table 3). In this case, averaging the contribution of ephemeral but strong fronts over time spreads their impact on the transport on longer intervals, causing the averaged currents to be overall slightly stronger and less variable. This highlights the risk of overestimating connectivity if submesoscale dynamics are not resolved in both space and time when the mean circulation is weak, and the submesoscale contribution to the currents is of a comparable magnitude.

Spatial averaging, on the other hand, compromises the representation of submesoscale fronts entirely and results in fewer and weaker links in the connectivity matrices, underscoring once more the importance of high spatial resolution in these types of studies. This effect was particularly evident during the 12-hr + Avg scenario, where only two links remained after averaging, and in the summer season, when most shallow coral species in the GoM spawn. Our results align with Dauhajre et al. (2019), indicating that coarser spatial resolutions may underestimate zonal and meridional fluxes in nearshore regions. Averaging in both space and time also leads to an overestimation of the offshore transport in both the FGBNMS and Pinnacles areas and in summer as well as winter.

Higher frequency forcing scenarios (30-min and 6-hr) did not show significant seasonal differences in the vertical distributions of particles in terms of means and extreme values. However, when averaging over times greater than 6 hr and over space, the vertical particle distributions tend to deepen. This is associated with an increase in material transport offshore, as the averaged currents become slightly stronger. This effect is particularly amplified in the Pinnacles area, where spatial averaging deepens the mean distribution even further due to the very steep

bathymetry. Taken together, our sensitivity analyses demonstrate the importance of capturing SCs at a high enough frequency (at least every 6 hr) to capture their impact on the potential connectivity (Sun et al., 2020; Vogt-Vincent et al., 2023).

5. Conclusions

In this work, we employed a physical modeling approach to establish a baseline for (a) how physical transport modulates the exchange of material at mesophotic depths in the northern GoM and (b) the minimum necessary model configuration to capture the impact of SCs on physical connectivity. We adopted a physical modeling approach consisting of coupling a regional ocean model (CROCO) and a Lagrangian tool (Ichthyop). Our goal was to provide insight into future conservation plans about critical areas and potential interconnections within the system, and the minimum requirements, in space and time, to adequately capture the impact of kilometer-scale circulations and their variability.

We focused on two environments, the areas of the FGBNMS and the Pinnacles Trend in the northern GoM, and found them largely isolated from each other at both seasonal and interannual scales. However, the presence of high variability linked with SCs allowed for occasional episodes of interchange from the Pinnacles area to the FGBNMS. Our results revealed overall year-round connectivity potential between mesophotic areas with no well-defined seasonal dependency. The lack of definite patterns was associated with the high intraseasonal variability of the flow field. Nevertheless, during both years of simulation, the largest number and the strongest connections, the longest dispersal distances, and the greater areas covered by particles consistently occurred in winter, contrasting with summer when the fewest and weakest links, shortest dispersal distances, and smallest areas were simulated. In the study areas, material dispersion appears to be primarily driven by the extension of shelf currents and the activity of submesoscale structures constrained by the 200-m isobath along the shelf edge, rather than by the larger mesoscale circulation.

The identified 3D connectivity was low even though the recruitment polygons are geographically close to each other, identifying depth as a key isolating factor in mesophotic environments and highlighting the need to include it in the design of MPAs. The smallest and northernmost areas, F1 and F4, which include Stetson Bank and Sonnier Bank, were found as the weakest sinks and, consequently, those with the least capacity to recover from environmental disturbances. We emphasize the need of marine planning strategies to prioritize the conservation of the mesophotic coral habitats on these banks.

Modeled connectivity metrics exhibited greater sensitivity to well-resolved SCs during the summer season, coinciding with the spawning period of many shallow-water coral species. The suppression of SCs, achieved by reducing flow variability by temporal averaging, resulted in an overestimation of connectivity and decreased zonal and meridional transport. In contrast, during winter, connectivity metrics remained more stable. Our findings underscore the necessity of high-resolution models (with horizontal grid spacing of 1 km or less and temporal resolution of 6 hr or less) to accurately simulate material transport processes in near-shelf areas.

Understanding the degree of connectivity between areas is crucial in designing effective and resilient MPAs and MPA networks. Through this work, we emphasize the need for high-resolution models, both spatially and temporally, to adequately resolve submesoscale processes and their variability. In the near future, we plan to explore if the transition from hydrostatic to nonhydrostatic models, which can better represent processes such as turbulent mixing and wave effects, may further enhance the capacity to conduct comprehensive connectivity analyses both between and within individual habitats.

Acknowledgments
This work was supported by the NOAA's National Centers for Coastal Ocean Science, Competitive Research Program, and Office of Ocean Exploration and Research under award NA18NOS4780166 titled ConnectivitY of CoraL Ecosystems (CYCLE) in the northwestern GoM and by the Deepwater Horizon oil spill Natural Resource Damage Assessment: Mesophotic and Deep Benthic Communities Habitat Assessment and Evaluation project, with grant funding through the National Marine Sanctuary Foundation, award 5300-23-03-045, to Lehigh University.

Data Availability Statement

CROCO ocean model and Ichtyop are open tools available at https://www.croco-ocean.org (Auclair et al., 2019) and https://ichthyop.org (Lett et al., 2008). Statistical analysis was done using Numpy and Pandas while Figures were made using Matplotlib, Scikit-learn, and Cartopy. Data to reproduce figures can be found at zenodo website (https://doi.org/10.5281/zenodo.14552232).

References

Amon, R. M. W., Ochoa, J., Candela, J., Herzka, S. Z., Pérez-Brunius, P., Sheinbaum, J., et al. (2023). Ventilation of the deep Gulf of Mexico and potential insights to the Atlantic Meridional Overturning Circulation. *Science Advances*, *9*(11). https://doi.org/10.1126/sciadv.ade1685

Auclair, F., Benshila, R., Bordois, L., Boutet, M., Brémond, M., Caillaud, M., et al. (2019). *Coastal and Regional Ocean COmmunity model* (Vol. 1.1). Zenodo.

Balbar, A. C., & Metaxas, A. (2019). The current application of ecological connectivity in the design of marine protected areas. *Global Ecology and Conservation*, *17*. e00569. https://doi.org/10.1016/j.gecco.2019.e00569

Barkan, R., Mcwilliams, J. C., Shchepetkin, A. F., Jeroen Molemaker, M., Renault, L., Bracco, A., & Choi, J. (2017). Submesoscale dynamics in the northern Gulf of Mexico. Part I: Regional and seasonal characterization and the role of river outflow. *Journal of Physical Oceanography*, *47*(9), 2325–2346. https://doi.org/10.1175/JPO-D-17

Bennett, M. J., Grupstra, C. G. B., Da-Anoy, J., Andres, M., Holstein, D., Rossin, A., et al. (2024). Ex situ spawning, larval development, and settlement in massive reef-building corals (Porites) in Palau. *Invertebrate Biology*, *143*(4). https://doi.org/10.1111/ivb.12447

Botsford, L. W., White, J. W., Coffroth, M. A., Paris, C. B., Planes, S., Shearer, T. L., et al. (2009). Connectivity and resilience of coral reef metapopulations in marine protected areas: Matching empirical efforts to predictive needs. *Coral Reefs*, *28*(2), 327–337. https://doi.org/10.1007/s00338-009-0466-z

Bracco, A., Choi, J., Joshi, K., Luo, H., & McWilliams, J. C. (2016). Submesoscale currents in the northern Gulf of Mexico: Deep phenomena and dispersion over the continental slope. *Ocean Modelling*, *101*, 43–58. https://doi.org/10.1016/j.ocemod.2016.03.002

Bracco, A., Choi, J., Kurian, J., & Chang, P. (2018). Vertical and horizontal resolution dependency in the model representation of tracer dispersion along the continental slope in the northern Gulf of Mexico. *Ocean Modelling*, *122*, 13–25. https://doi.org/10.1016/j.ocemod.2017.12.008

Bracco, A., Liu, G., Galaska, M. P., Quattrini, A. M., & Herrera, S. (2019). Integrating physical circulation models and genetic approaches to investigate population connectivity in deep-sea corals. *Journal of Marine Systems*, *198*, 103189. https://doi.org/10.1016/j.jmarsys.2019.103189

Cairns, S., & Bayer, F. (2009). Chapter 13. Octocorallia (Cnidaria) of the Gulf of Mexico. *Gulf of Mexico-Origins, Waters, and Biota*, *1*, 321–331.

Cardona, Y., & Bracco, A. (2016). Predictability of mesoscale circulation throughout the water column in the Gulf of Mexico. *Deep-Sea Research Part II Topical Studies in Oceanography*, *129*, 332–349. https://doi.org/10.1016/j.dsr2.2014.01.008

Cardona, Y., Ruiz-Ramos, D. V., Baums, I. B., & Bracco, A. (2016). Potential connectivity of coldwater black coral communities in the northern Gulf of Mexico. *PLoS One*, *11*(5), e0156257. https://doi.org/10.1371/journal.pone.0156257

Cummings, J. A. (2006). Operational multivariate ocean data assimilation. *Quarterly Journal of the Royal Meteorological Society*, *131*(613), 3583–3604. https://doi.org/10.1256/qj.05.105

Cummings, J. A., & Smedstad, O. M. (2013). Variational data assimilation for the global ocean. In *Data assimilation for atmospheric, oceanic and hydrologic applications* (Vol. III, pp. 303–343). https://doi.org/10.1007/978-3-642-35088-7_13

D'Asaro, E. A., Carlson, D. F., Chamecki, M., Harcourt, R. R., Haus, B. K., Fox-Kemper, B., et al. (2020). Advances in observing and understanding small-scale open ocean circulation during the Gulf of Mexico Research Initiative Era. *Frontiers in Marine Science*, *7*. https://doi.org/10.3389/fmars.2020.00349

Dauhajre, D. P., McWilliams, J. C., & Renault, L. (2019). Nearshore Lagrangian connectivity: Submesoscale influence and resolution sensitivity. *Journal of Geophysical Research: Oceans*, *124*(7), 5180–5204. https://doi.org/10.1029/2019JC014943

Dee, S. G., Torres, M. A., Martindale, R. C., Weiss, A., & DeLong, K. L. (2019). The future of reef ecosystems in the Gulf of Mexico: Insights from coupled climate model simulations and ancient hot-house reefs. *Frontiers in Marine Science*, *6*. https://doi.org/10.3389/fmars.2019.00691

Denton, S.-, Cryer, E., Gocke, P. F., Harrelson, J. P., Kinsella, M. R., Pulver, D. L., et al. (2011). Descriptions of the U.S. Gulf of Mexico reef fish bottom longline and vertical line fisheries based on observer data. http://hdl.handle.net/1834/26270

de Oliveira Soares, M., de Araújo, J. T., Ferreira, S. M. C., Santos, B. A., Boavida, J. R. H., Costantini, F., & Rossi, S. (2020). Why do mesophotic coral ecosystems have to be protected? *Science of the Total Environment*, *726*. https://doi.org/10.1016/j.scitotenv.2020.138456

Egbert, G. D., & Erofeeva, S. Y. (2002). Efficient inverse modeling of barotropic ocean tides. *Journal of Atmospheric and Oceanic Technology*, *19*(2), 183–204. https://doi.org/10.1175/1520-0426(2002)019<0183:eimobo>2.0.co;2

Freeman, L. A., Kleypas, J. A., & Miller, A. J. (2013). Coral reef habitat response to climate change scenarios. *PLoS One*, *8*(12), e82404. https://doi.org/10.1371/journal.pone.0082404

Garavelli, L., Studivan, M. S., Voss, J. D., Kuba, A., Figueiredo, J., & Chérubin, L. M. (2018). Assessment of mesophotic coral ecosystem connectivity for proposed expansion of a marine sanctuary in the Northwest Gulf of Mexico: Larval dynamics. *Frontiers in Marine Science*, *5*(MAY). https://doi.org/10.3389/fmars.2018.00174

Gil-Agudelo, D. L., Cintra-Buenrostro, C. E., Brenner, J., González-Díaz, P., Kiene, W., Lustic, C., & Pérez-España, H. (2020). Coral reefs in the Gulf of Mexico large marine ecosystem: Conservation status, challenges, and opportunities. *Frontiers in Marine Science*, *6*. https://doi.org/10.3389/fmars.2019.00807

Gittings, S. R., Bright, T. J., Schroeder, W. W., Sager, W. W., Laswell, J. S., & Rezak, R. (1992). Invertebrate assemblages and ecological controls on topographic features in the northeast Gulf of Mexico. In *Bulletin of marine science* (Vol. 50(3)).

Green, A., White, A., Kilarski, S., Fernandes, L., Tanzer, J., Aliño, P. M., et al. (2013). Designing marine protected area networks to achieve fisheries, biodiversity, and climate change objectives in tropical ecosystems: A practitioner guide This publication was produced and printed with support from the United States Agency for International Development's regional Asia program through the Coral Triangle Support Partnership.

Haza, A. C., Özgökmen, T. M., & Hogan, P. (2016). Impact of submesoscales on surface material distribution in a Gulf of Mexico mesoscale eddy. *Ocean Modelling*, *107*, 28–47. https://doi.org/10.1016/j.ocemod.2016.10.002

Jordan, A. C. (2018). *Patterns in Caribbean coral spawning*. Nova Southern University.

Klein, C. J., Ban, N. C., Halpern, B. S., Beger, M., Game, E. T., Grantham, H. S., et al. (2010). Prioritizing land and sea conservation investments to protect coral reefs. *PLoS One*, *5*(8), e12431. https://doi.org/10.1371/journal.pone.0012431

Lawman, A. E., Dee, S. G., DeLong, K. L., & Correa, A. M. S. (2022). Rates of future climate change in the Gulf of Mexico and the Caribbean Sea: Implications for coral reef ecosystems. *Journal of Geophysical Research: Biogeosciences*, *127*(9). https://doi.org/10.1029/2022JG006999

Lett, C., Verley, P., Mullon, C., Parada, C., Brochier, T., Penven, P., & Blanke, B. (2008). A Lagrangian tool for modelling ichthyoplankton dynamics. *Environmental Modelling & Software*, *23*(9), 1210–1214. https://doi.org/10.1016/j.envsoft.2008.02.005

Levin, N., Kark, S., & Danovaro, R. (2018). Adding the third dimension to marine conservation. *Conservation Letters*, *11*(3). https://doi.org/10.1111/conl.12408

Liu, G., Bracco, A., Quattrini, A. M., & Herrera, S. (2021). Kilometer-scale larval dispersal processes predict metapopulation connectivity pathways for Paramuricea biscaya in the northern Gulf of Mexico. *Frontiers in Marine Science*, *8*. https://doi.org/10.3389/fmars.2021.790927

Liu, G., Bracco, A., & Sitar, A. (2021). Submesoscale mixing across the mixed layer in the Gulf of Mexico. *Frontiers in Marine Science*, *8*. https://doi.org/10.3389/fmars.2021.615066

Liu, G., Falasca, F., & Bracco, A. (2021). Dynamical characterization of the loop current attractor. *Geophysical Research Letters*, *48*(24). https://doi.org/10.1029/2021GL096731

Locker, S. D., Armstrong, R. A., Battista, T. A., Rooney, J. J., Sherman, C., & Zawada, D. G. (2010). Geomorphology of mesophotic coral ecosystems: Current perspectives on morphology, distribution, and mapping strategies. *Coral Reefs*, *29*(2), 329–345. https://doi.org/10.1007/s00338-010-0613-6

Łuczyński, P., Skompski, S., & Zapalski, M. K. (2023). Mesophotic vs. shallow water reefs: Ecosystem connectivity in the Silurian of Gotland. *Coral Reefs*, *42*(5), 1147–1161. https://doi.org/10.1007/s00338-023-02416-1

Luo, H., Bracco, A., Cardona, Y., & McWilliams, J. C. (2016). Submesoscale circulation in the northern Gulf of Mexico: Surface processes and the impact of the freshwater river input. *Ocean Modelling*, *101*, 68–82. https://doi.org/10.1016/j.ocemod.2016.03.003

McWilliams, J. C. (2016). Submesoscale currents in the ocean. *Proceedings of the Royal Society A: Mathematical, Physical and Engineering Sciences*, *472*(2189), 20160117. https://doi.org/10.1098/rspa.2016.0117

NOAA National Centers for Environmental Information. (2006). NOAA National Geophysical Data Center. 2006: 2-minute Gridded Global Relief Data (ETOPO2) v2.

Poje, A. C., Özgökmen, T. M., Lipphardt, B. L., Haus, B. K., Ryan, E. H., Haza, A. C., et al. (2014). Submesoscale dispersion in the vicinity of the Deepwater Horizon spill. *Proceedings of the National Academy of Sciences of the United States of America*, *111*(35), 12693–12698. https://doi.org/10.1073/pnas.1402452111

Quigley, C. N., Roughan, M., Chaput, R., Jeffs, A. G., & Gardner, J. P. A. (2022). Combined biophysical and genetic modelling approaches reveal new insights into population connectivity of New Zealand green-lipped mussels. *Frontiers in Marine Science*, *9*. https://doi.org/10.3389/fmars.2022.971209

Raitsos, D. E., Brewin, R. J. W., Zhan, P., Dreano, D., Pradhan, Y., Nanninga, G. B., & Hoteit, I. (2017). Sensing coral reef connectivity pathways from space. *Scientific Reports*, *7*(1), 9338. https://doi.org/10.1038/s41598-017-08729-w

Rezak, R., Bright, T., & McGrail, D. (1983). Reefs and banks of the northwestern Gulf of Mexico: Their geological, biological, and physical dynamics.

Rocha, L. A., Pinheiro, H. T., Shepherd, B., Papastamatiou, Y. P., Luiz, O. J., Pyle, R. L., & Bongaerts, P. (2018). Mesophotic coral ecosystems are threatened and ecologically distinct from shallow water reefs. *Science*, *361*(6399), 281–284. https://doi.org/10.1126/science.aaq1614

Rodrigues, L. J., & Padilla-Gamiño, J. L. (2022). Trophic provisioning and parental trade-offs lead to successful reproductive performance in corals after a bleaching event. *Scientific Reports*, *12*(1), 18702. https://doi.org/10.1038/s41598-022-21998-4

Romero, L., Uchiyama, Y., Carter, O. J., Mcwilliams, J. C., & Siegel, D. A. (2013). Simulations of nearshore particle-pair dispersion in southern California. *Journal of Physical Oceanography*, *43*(9), 1862–1879. https://doi.org/10.1175/JPO-D-13-011.1

Saint-Amand, A., Lambrechts, J., & Hanert, E. (2023). Biophysical models resolution affects coral connectivity estimates. *Scientific Reports*, *13*(1), 9414. https://doi.org/10.1038/s41598-023-36158-5

Sanvicente-Añorve, L., Zavala-Hidalgo, J., Allende-Arandía, E., & Hermoso-Salazar, M. (2018). Larval dispersal in three coral reef decapod species: Influence of larval duration on the metapopulation structure. *PLoS One*, *13*(3), e0193457. https://doi.org/10.1371/journal.pone.0193457

Sheehan, E. V., Holmes, L. A., Davies, B. F. R., Cartwright, A., Rees, A., & Attrill, M. J. (2021). Rewilding of protected areas enhances resilience of marine ecosystems to extreme climatic events. *Frontiers in Marine Science*, *8*. https://doi.org/10.3389/fmars.2021.671427

Sherman, K., & Alexander, L. (1986). Variability and management of large marine ecosystems. *Natural Resources*.

Silva, M., Etnoyer, P. J., & MacDonald, I. R. (2016). Coral injuries observed at Mesophotic Reefs after the Deepwater Horizon oil discharge. *Deep-Sea Research Part II Topical Studies in Oceanography*, *129*, 96–107. https://doi.org/10.1016/j.dsr2.2015.05.013

Slattery, M., Lesser, M. P., Brazeau, D., Stokes, M. D., & Leichter, J. J. (2011). Connectivity and stability of mesophotic coral reefs. *Journal of Experimental Marine Biology and Ecology*, *408*(1–2), 32–41. https://doi.org/10.1016/j.jembe.2011.07.024

Spies, R. B., Senner, S., & Robbins, C. S. (2016). An overview of the northern Gulf of Mexico ecosystem. *Gulf of Mexico Science*, *33*(1), 98–121. https://doi.org/10.18785/goms.3301.09

Stephenson, F., Bulmer, R. H., Meredyth-Young, M., Meysick, L., Hewitt, J. E., & Lundquist, C. J. (2019). Effects of benthic protection extent on recovery dynamics of a conceptual seafloor community. *Frontiers in Marine Science*, *6*(SEP). https://doi.org/10.3389/fmars.2019.00607

Studivan, M. S., & Voss, J. D. (2018). Assessment of mesophotic coral ecosystem connectivity for proposed expansion of a Marine sanctuary in the Northwest Gulf of Mexico: Population genetics. *Frontiers in Marine Science*, *5*(MAY). https://doi.org/10.3389/fmars.2018.00152

Sullivan-Stack, J., Aburto-Oropeza, O., Brooks, C. M., Cabral, R. B., Caselle, J. E., Chan, F., et al. (2022). A scientific synthesis of marine protected areas in the United States: Status and recommendations. *Frontiers in Marine Science*, *9*. https://doi.org/10.3389/fmars.2022.849927

Sun, D., Bracco, A., Barkan, R., Berta, M., Dauhajre, D., Jeroen, M., et al. (2020). Diurnal cycling of submesoscale dynamics: Lagrangian implications in drifter observations and model simulations of the Northern Gulf of Mexico. *Journal of Physical Oceanography*, *50*(6), 1605–1623. https://doi.org/10.1175/jpo-d-19-0241.1

Sun, D., Bracco, A., & Liu, G. (2022). The role of freshwater forcing on surface predictability in the Gulf of Mexico. *Journal of Geophysical Research: Oceans*, *127*(5). https://doi.org/10.1029/2021JC018098

Turner, E. R., & Rabalais, N. N. (2018). The gulf of Mexico. In *World seas: An environmental evaluation Volume I: Europe, the Americas and west Africa* (pp. 445–464). Elsevier. https://doi.org/10.1016/B978-0-12-805068-2.00022-X

Uchiyama, Y., Idica, E. Y., McWilliams, J. C., & Stolzenbach, K. D. (2014). Wastewater effluent dispersal in Southern California Bays. *Continental Shelf Research*, *76*, 36–52. https://doi.org/10.1016/j.csr.2014.01.002

Viehman, T. S., Reguero, B. G., Lenihan, H. S., Rosman, J. H., Storlazzi, C. D., Goergen, E. A., et al. (2023). Coral restoration for coastal resilience: Integrating ecology, hydrodynamics, and engineering at multiple scales. *Ecosphere*, *14*(5). https://doi.org/10.1002/ecs2.4517

Vogt-Vincent, N. S., Mitarai, S., & Johnson, H. L. (2023). High-frequency variability dominates potential connectivity between remote coral reefs. *Limnology & Oceanography*, *68*(12), 2733–2748. https://doi.org/10.1002/lno.12455

Zavala-Hidalgo, J., Romero-Centeno, R., Mateos-Jasso, A., Morey, S. L., & Martínez-López, B. (2014). The response of the Gulf of Mexico to wind and heat flux forcing: What has been learned in recent years? *Atmósfera*, *27*(3), 317–334. https://doi.org/10.1016/s0187-6236(14)71119-1

Zeng, X., Li, Y., & He, R. (2015). Predictability of the Loop Current variation and eddy shedding process in the Gulf of Mexico using an artificial neural network approach. *Journal of Atmospheric and Oceanic Technology*, *32*(5), 1098–1111. https://doi.org/10.1175/JTECH-D-14-00176.1

Zhang, B. D., Li, Y. L., Xue, D. X., & Liu, J. X. (2020). Population genomics reveals shallow genetic structure in a connected and ecologically important fish from the northwestern Pacific Ocean. *Frontiers in Marine Science*, *7*. https://doi.org/10.3389/fmars.2020.00374

Zhang, Y., & Hu, C. (2021). Ocean temperature and color frontal zones in the Gulf of Mexico: Where, when, and why. *Journal of Geophysical Research: Oceans*, *126*(10). https://doi.org/10.1029/2021JC017544

Zhang, Z., Zhang, X., Qiu, B. O., Zhao, W., Zhou, C., Huang, X., & Tian, J. (2021). Submesoscale currents in the subtropical upper ocean observed by long-term high-resolution mooring arrays. *Journal of Physical Oceanography*, *51*(1), 187–206. https://doi.org/10.1175/JPO-D-20-0100.s1

Zhao, L., Qu, F., Song, N., Han, Z., Gao, T., & Zhang, Z. (2021). Population genomics provides insights into the population structure and temperature-driven adaptation of Collichthys lucidus. *BMC Genomics*, *22*(1), 729. https://doi.org/10.1186/s12864-021-08045-8

Zhong, Y., & Bracco, A. (2013). Submesoscale impacts on horizontal and vertical transport in the Gulf of Mexico. *Journal of Geophysical Research: Oceans*, *118*(10), 5651–5668. https://doi.org/10.1002/jgrc.20402

Zhou, X., Lopera, L., Roa-Varón, A., & Bracco, A. (2024). Modeling the larval dispersal and connectivity of Red Snapper (Lutjanus campechanus) in the Northern Gulf of Mexico. *Progress in Oceanography*, *224*, 103265. https://doi.org/10.1016/j.pocean.2024.103265

Zhu, Y., & Liang, X. (2022). Characteristics of Eulerian mesoscale eddies in the Gulf of Mexico. *Frontiers in Marine Science*, *9*. https://doi.org/10.3389/fmars.2022.1087060